Wayne State University Dissertations

1-1-2015

Effect Of Impact Damage On Compression-Compression Fatigue Behavior Of Sandwich Composites

Ali M. Al-Sharif
Wayne State University,

Recommended Citation

EFFECT OF IMPACT DAMAGE ON COMPRESSION-COMPRESSION FATIGUE BEHAVIOR OF SANDWICH COMPOSITES

by

ALI M. AL-SHARIF

DISSERTATION

Submitted to the Graduate School

of Wayne State University,

Detroit, Michigan

in partial fulfillment of the requirements

for the degree of

DOCTOR OF PHILOSOPHY

2015

MAJOR: MECHANICAL ENGINEERING

Approved by:

_____
Advisor   Date

_____

_____

_____

DEDICATION

To my parents who had me in all their prayers.

To my beloved wife and my daughter, Kadeeja, for their support and patience during my

Ph.D. study.

To all of my brothers and sisters for their encouragement and support.

ACKNOWLEDGMENTS

TABLE OF CONTENTS

LIST OF TABLES

LIST OF FIGURES

CHAPTER ONE

INTRODUCTION

1.1 The Composite Sandwich Concept

A composite material is composed mainly of two or more constituent materials combined in such a way that the resulting material has more useful applications than the constituent materials alone. The constituent materials play a key role in the development of the final composite material properties. Most composites have two constituent materials: a matrix and reinforcement. The matrix is the component that holds the reinforcement together to form the bulk of the material, and the reinforcement is usually much stronger and stiffer compared to the matrix, and gives the composite its excellent properties. Advanced composite materials used in structural applications are obtained by reinforcing a matrix material with continuous fibers having high strength and stiffness properties. For any application, the selection of a composite material always involves selection of reinforcing fiber and matrix, and their fractional volume in the resulting material. A lamina is defined as a thin layer which is composed of at least two different materials that are bonded together and it is the basic building block of a laminate. Laminated composite materials is a bonded stack of lamina with various orientation of principle material directions in lamina [1].

A sandwich panel is classified as a special form of a laminated composite structure; it is composed of two thin composite laminates (face sheets) having high

strength and stiffness and they are bonded adhesively with a low density core material located in between them. The ASTM defines a sandwich structure as follows:

"A structural sandwich is a special form of a laminated composite comprising of a combination of different materials that are bonded to each other so as to utilize the properties of each separate component to the structural advantage of the whole assembly". Three main parts of the structural sandwich panel including adhesive joints, high strength facings and a low density core material are illustrated in Fig. 1.1.
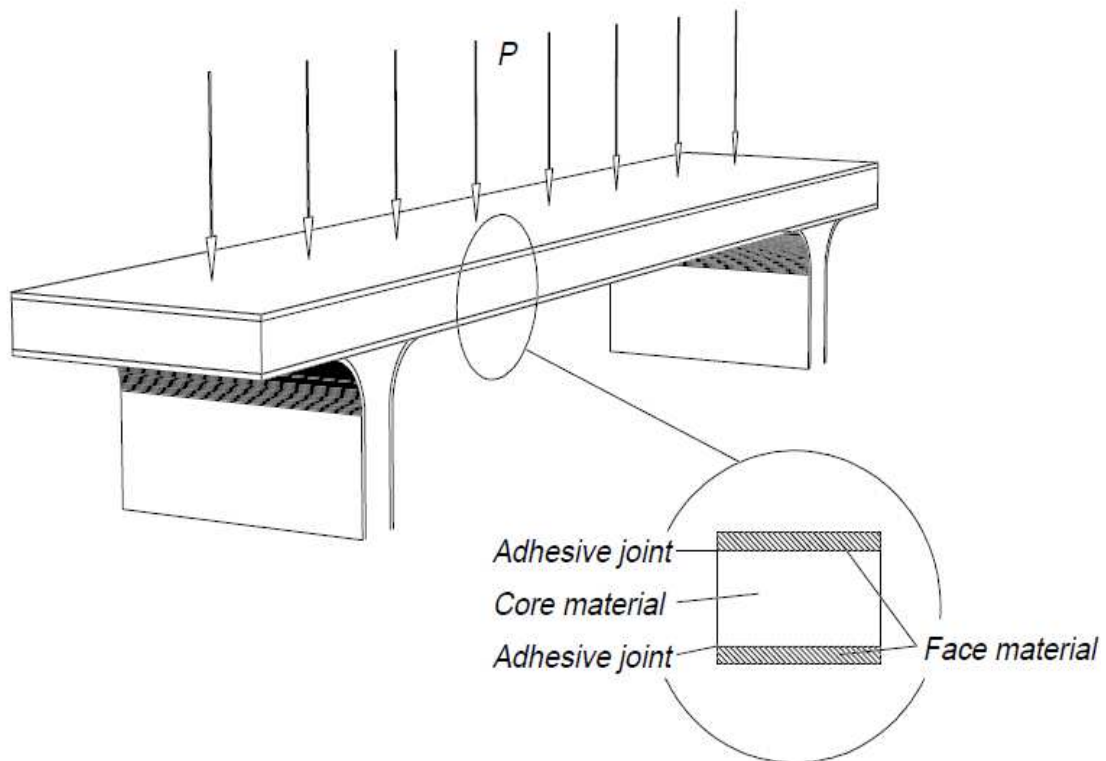
Fig. 1.1. Schematic of a structural sandwich panel [2]

1.2 The Composite Sandwich Components

In a sandwich structure, the main function of the adhesive attachment is to rigidly bond two thin stiff face sheets and a thick weaker core together in order to form an efficient load carrying assembly (Fig.1) and transmit axial and shear loads between three components of this structure. The bond must be strong enough to get rigid adhesion between these facings and the core material in order to resist shear and tensile stresses set up between them. In general, the bond strength should be greater than the core strength to avoid the interface failure between the core and skin. The external bending moment is counteracted by an efficient stress couple formed by acting of the skins where one skin is subjected to compression and the other skin is subjected to tension. The core separates the skins, carries loads from one skin to the other, resists shear loads, and stabilizes the skins against bending and buckling. Traditionally, light-weight core materials, such as foam core, truss core, honeycomb core, and balsa wood have been used in fabricating sandwich structures. The advantages of the structural composite sandwich design are high stiffness and strength to weight ratios, high flexural rigidity, high energy absorbing capability, excellent resistance to corrosion and good acoustic and thermal insulation [2].

Composite sandwich structures consist of components in the form of plates and beams. The sandwich beam is one of the most common composite structures that uses largely in different applications due to the extremely flexural stiffness-to-weight ratios and flexural strength-to-weight ratios resulting from the load carrying

faces being separated by the core. These advantages including high bending stiffness and low specific weight are enhanced by the introduction of fiber reinforced composite laminates for the faces. The composite sandwich beam works in similar manner as an I-beam where faces correspond to flanges and the core corresponds to the web as represented in Fig. 1.2. The difference is that the faces of a sandwich structure are of different materials from the core and they are held by the core which is spread out as a continuous support rather than concentrated in a narrow web [2].
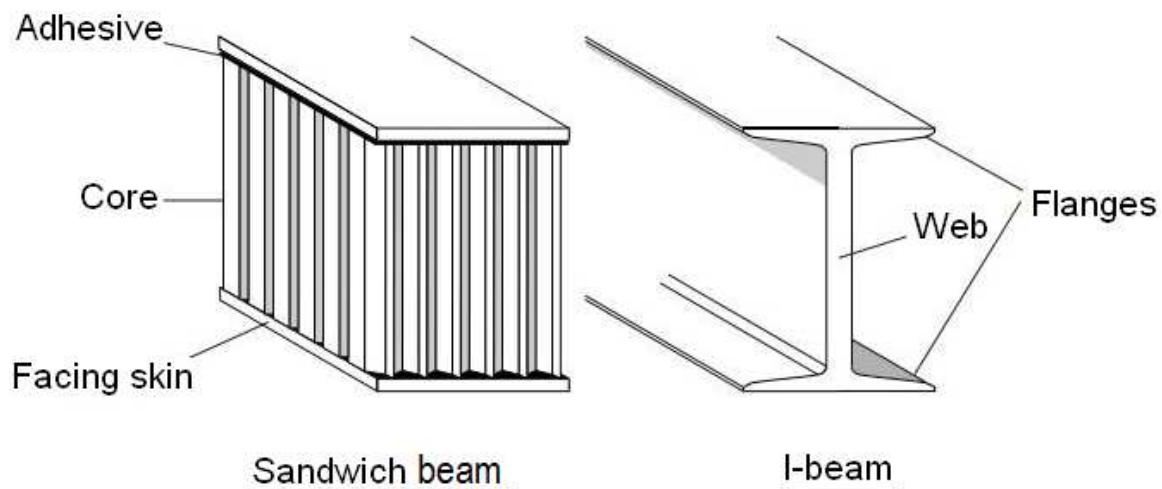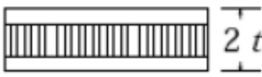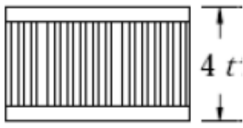
Fig. 1.2. Sandwich beam and I beam [2]

The typical beam theory with typical values for the skin and core is used to compare the flexural strength and stiffness of the solid laminate panels and

composite sandwich panels. The weight, bending stiffness and the strength of the solid laminate are calculated and set them to unity. By supposing the laminate is split in two halves and separated with a core to form a sandwich structure, and this separation is done without adding substantial weight to the entire structure. The stiffness and strength of the sandwich panel is found to be much greater than the solid laminate. The comparative flexural strength and stiffness of the solid laminate and composite sandwich panels is given in Table 1.1. The comparison shows that the flexural stiffness and strength of a sandwich structure can be enhanced by increasing the core thickness which increases the moment of inertia of the structure with little increase in weight.

Table 1.1. An example of Structural efficiency of honeycomb sandwich panels in terms of weight [3]

	Solid material	Core thickness t	Core thickness 3t
	t	$2\,t$	$4\,t$
Bending stiffness	1.0	7.0	37.0
Bending strength	1.0	3.5	9.2
Weight	1.0	1.03	1.06

Earlier the composite materials in the form of composite laminates or sandwich composites were only limited to aerospace industry due to its high cost and manufacturing difficulties. Invent of new low cost materials and understanding of their mechanical behavior under various conditions allows to see composites in extensive applications in Industries. The use of sandwich composites is rapidly increasing in many fields, such as aerospace, automobiles, ships, wind energy systems, and other advanced structural applications due to their high strength and stiffness to weight ratios and the ease of manufacturing.

1.3 The Sandwich Composite Materials

The design of composite structures consisting of components in the form of beams, plates, shells, grids, and sandwich panels is just as much as materials selection problem as sizing problem. Nowadays, a variety of materials are used as faces and cores in sandwich structures. The increase availability of material choices may seem an additional complexity but has made it is possible to use these light stiff and strong materials in the constructions of modern industrial applications. For structural purposes, the material selection plays a very important role in engineering design by considering some factors such as strength, stiffness, adhesive performance, environmental behavior, economic availability etc.

1.3.1 Face Materials

The weight of the structure is very important in many applications as aerospace and automotive structures. The material having a high strength-to-weight ratio or a high stiffness-to-weight ratio should be used when the structural design is strength critical or stiffness critical. To form composite, the reinforcing fibers are combined with a matrix material which leads to some reduction in the tremendously high specific strengths and specific moduli, but composite materials still offer low density along with higher strength properties than metals except the stiffness which is generally lower [4]. In sandwich panels, high performance materials are considered for the facings providing flexural strength and impact resistance to the sandwich structure. The face materials are mainly categorized into metallic and non-metallic materials. Conventional metals such as steel, stainless steel and aluminum are often used for the face material. In many applications, reinforcing fibers including glass, carbon, kevlar, boron, silicon carbide, bio-based fibers including flax and hemp etc. are also chosen to be as facings. The properties for some of these materials are listed in Table 1.2.

1.3.2 Core

In a composite sandwich structure, the core serves to carry and hold the upper and lower face sheets in positions far away from neutral axis, therefore it has to be stiff enough to keep constant distance between the facings. It also resists

Table 1.2. Typical mechanical properties for some of face materials [2]

Material	ρ (kg/m^3)	E (GPa)	σ_u (MPa)
Metals:			
Stainless steel	7900	196	200
Aluminum Alloy	2700	73	300
Titanium alloy	4500	108	980
Non-metals			
Kevlar/Epoxy (Unidirectional)	1300	76/6	1400/12
Glass/Epoxy (Unidirectional)	1800	39/8	1060/30
Carbon/Epoxy (Unidirectional)	1600	180/10	1500/40
E-glass/Epoxy (Bi-directional)	1800	20	550
Kevlar/Polyester (Bi-directional)	1300	17.5	375
Glass weave/Polyester (Bi-directional)	1700	16	250

transverse shear and provides other functions such as absorbing energy and insulating heat transfer. The first material utilized as a core in sandwich structures is balsa wood, and it is still used in Marine industry, wind turbine blades, and structural composite panels. Balsa wood shows a high-aspect ratio closed cell structure under the microscope. The properties of balsa with water content decline rapidly due to the sensitivity to humidity. To conquer this problem the shape of balsa in most common utilized in sandwich structures is end-grain. The balsa wood

is cut up into cubic pieces and bonded together to produce a block of end-grain where the fiber or grain is oriented along thickness of the sheet as shown in Fig. 1.3(a). End-grain balsa has high strength to weight ratio, and it has natural resistance to rot and mold. Honeycomb core material has been used in aerospace applications and developed to provide high shear strength, and stiffness-to-weight ratio. The majority of honeycomb core is air as shown in Fig. 1.3(b), and this perhaps makes it the lightest material. The honeycomb core is more expensive then the end-grain balsa core material. Cellular foam core material (Fig. 1.3(c)) can be used in composite structures, and it has lower stiffness and strength to weight. The foam core is less expensive than honeycomb, and it is easy to manufacture and bond to the skins. In addition, the cellular foams offer high thermal insulation and acoustic damping, and they are impervious to moisture [2]. Table 1.3 summarizes some of the common core materials used in industrial applications.
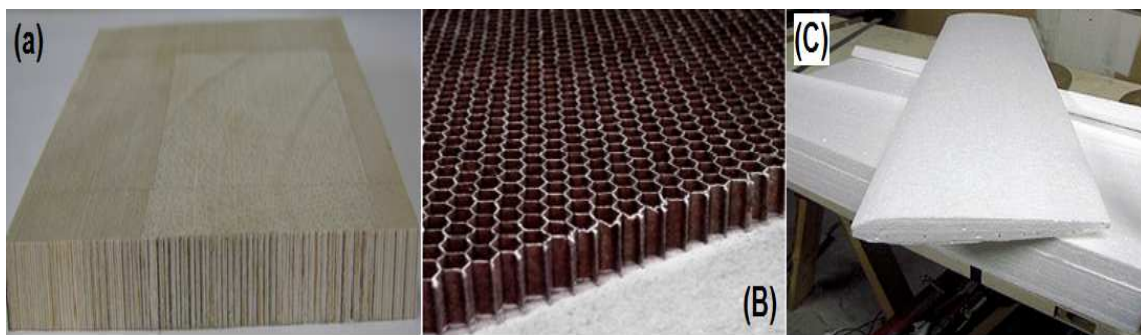
Fig. 1.3. Some types of core materials: (a) Honeycomb; (b) Balsa wood; and (c) Cellular foam

Table 1.3. Typical mechanical properties of some core materials [2]

Material (Density, kg/m^3)	Gc (MPa)	σ_u (MPa)
Balsa wood (96)	72.85/12.5	10.1/0.81
Honeycomb:		
Aluminum alloy (92)	620/260	3.1/2.0
Aluminum alloy (130)	930/370	5.0/3.1
Nomex honeycomb (80)	69/44	2.2/1.0
Paper honeycomb (56)	141/38	1.3/0.48
Cellular Foam:		
Polyurethane (40)	4	0.25
Polystyrene (60)	20	0.6
Polyvinyl chloride (80)	31	1.0

1.4 Fabrication of Composites

It is very important for us to know how composites materials are manufactured because the selection of a fabrication method for a particular component as a part of the composite structure will depend on the structural material itself, the part design and its application. The constituent materials play an important role to select a fabrication process in the composite, and the key of this selection is the matrix type in the lamina structure. In this section, brief information will only cover some of those fabrication processes (i.e., one of these

processes is the vacuum press molding used for making sandwich panels for this research) utilized for polymer matrix composites and a summary of fabrication processes with various types of fibers reinforcement is given in Table 1.4. The processes contain some form of molding; a mold tool is used to give the resin and fibers combination the desired shape prior to and during cure. Two open mold processes such as hand lay-up of woven fiber mat or chopped strand mat (Fig. 1.4(a)) and spray-up of chopped fibers shown in Fig 1.4(b) is utilized to develop the work, fabricate prototype, and produce large components in relatively small quantities [4]. Molding operations can begin either with hand or automated deposition of preimpregnated fibers in layers. The prepreg layers (prepreg tape is composed of fibers saturated or coated with resinous material such as epoxy) are often precut. Subsequently, laying-up the tape at the required orientation on the mold, stacking layers in the required stacking sequence and then compressing the layers under elevated temperature to form the final laminate. The fabricator with prepreg layers no longer has to concern about how to combine the resin with the fibers in the correct way, and the hot mold-melt process (Fig. 1.5) was used to make most prepreg tape. The resin is incompletely cured if a thermosetting risen is used and the tape must be kept in the fridge to avoid full curing until final use. If the tape consisting of thermoplastic resin is used, then the tape can be stored at room temperature until it is heated during manufacturing [4].

There are different manufacturing techniques which can be used to fabricate composite Sandwich panels. They include adhesive bonding, Liquid

molding, continuous lamination, vacuum bag and autoclave molding. A sandwich structure with prepreg tape will have the same technique that used to form the laminate structure. The most basic fabricating process for the sandwich structure is adhesive bonding. In this process, the adhesive layers are inserted between the facings and core and then the structure is subjected to the required temperature and pressure for curing. To obtain strong and rigid adhesion, the bond surface should be rugged and abraded.

Autoclave molding is the standard process in aerospace industry and it is used for composite fabrication with prepreg tape as shown in Fig. 1.6. To cure samples for this research work, a vacuum press molding (Autoclave type) is utilized for making composite sandwich panels. The prepreg tape is cut to the desired shape and laid up directly onto each side of the core in the mold, and then the mold and lay-up are placed in a vacuum chamber and subjected to the required temperature and pressure for curing. The mold and lay-up are often coated with a mold release which prevents bonding of the risen and matrix material to the mold. The curing temperature and applied pressure are controlled for prescribed period of time for resin cross-linking and temperature is gradually decreased after curing. The Fabrication process for composite sandwich panels by using the vacuum chamber surrounding the platen-mold assembly will reduce the void contents in the cured laminate.

Table. 1.4. Fabrication processes for polymer Matrix composites [4]

Process	Type of Reinforcement			
	Continuous	Chopped	Woven	Hybrid
Open mold				
Hand lay-up		X	X	
Spray-up		X		
Autoclave	X		X	
Compressing molding	X	X	X	X
Filament winding	X			
Roll-wrapping	X		X	
Pultrusion	X		X	
Liquid composite molding	X	X	X	
Reinforced reaction injection molding		X		
Resin infusion	X	X	X	X
Automated fiber placement	X		X	
Thermoplastic molding	X	X	X	X
Programmable powdered perform process		X		
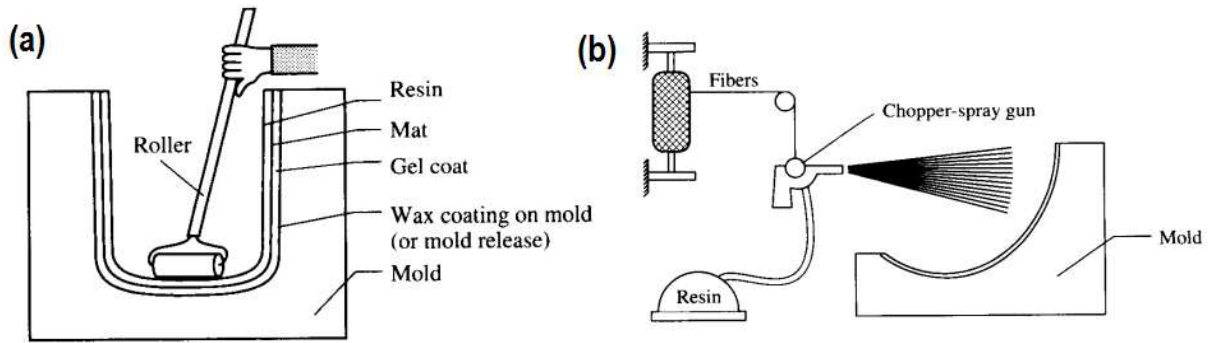
Fig. 1.4 Open mold compsite fabrication: (a) hand lay-up and (b) spray-up [4]
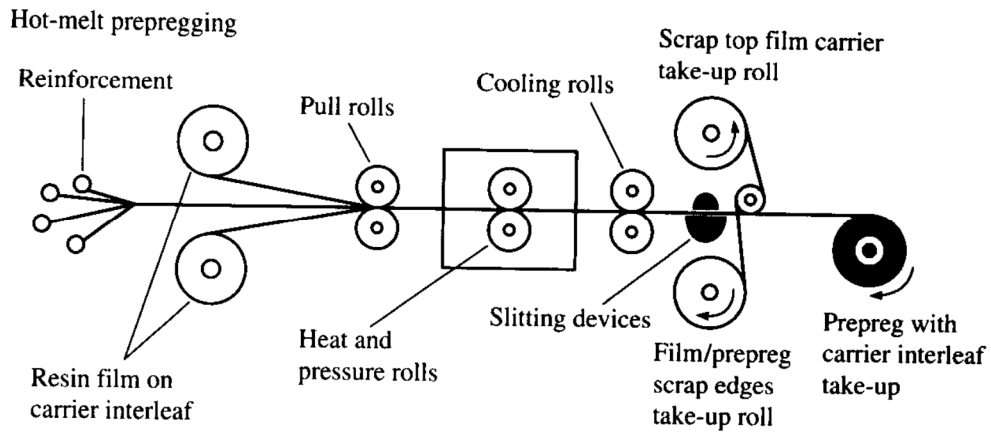
Fig. 1.5. Hot-melt prepregging process [4]
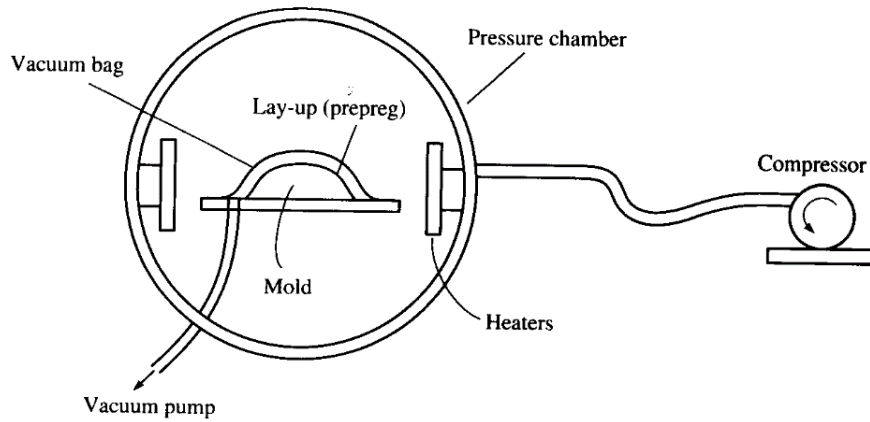
Fig. 1.6. Autoclave Molding [4]

1.5 Low Velocity Impact and Buckling Behavior of Sandwich Composites

Considerable attention is being focused on understanding the effect of impact damage on such sandwich composites (SC). Low velocity impact damage can take place in composites when the objects, such as hand tools and runway debris fall down on composites. It can even occur in composites that used in vehicles when they are hit by stones from the ground. The excellent mechanical properties of the composite materials can be severely reduced whether or not the impact damage is detectable by visual inspection. The consequence of low-velocity impact causes that two adjacent layers become to partially debond at their interface due to the formation of internal delaminated zones. In sandwich structures, the delamination laying occur along the interface between the faces and core and it may occur due to a variety of reasons such as low energy impact, manufacturing defects, high stress concentration at geometric or material discontinuities. Delamination in composite structures can be serious threat to the safety of the structure, and it leads to loss its stiffness and strength under some conditions. The compression after impact (CAI) testing data plays an important role in composite structures design because of the strength reduction of these composites.

The debonded sandwich panels in the form of beams and plates are susceptible to buckling under in-plane compressive loads, which may lead to the propagation of the delamination, and then follow by core and/or face-sheet failure. Due to the presence of delaminated area, the designed buckling strength of the

composite sandwich structures can be reduced when it is subjected to the compressive loading. Since buckling of sandwich structures can lead to a catastrophic failure, it must be taken into account in design and analysis of these structures.

1.6 Compression-Compression Fatigue of Sandwich Composites

The sandwich structures are subjected to vibration or cyclic loading when these structures have been utilized in transport industries. The fatigue resistance and the associated failure modes under various stresses are very important to be understood. Fatigue strength of sandwich materials under compression, tensile, and flexural stress states are significant prior to using these materials in different structural applications. It is difficult to predict the post-impact fatigue damage because a variety of failure modes can be seen. The fatigue damage appears in different forms including delamination, core shear, matrix cracking, and fiber breakage. The fatigue performance and the growth of local delamination induced by impact in the sandwich beam which subjected to compression-compression fatigue are also very important to be determined for the designed composite sandwich structures in order to meet design requirements in different industrial applications.

CHAPTER TWO

LITERATURE REVIEW AND OBJECTIVES

2.1 Literature Review

2.1.1 Buckling of Delaminated Sandwich Composites

Delamination appears in laminated composite materials due to manufacturing errors including imperfect curing process or in-service accident such as a low velocity impact. Due to the presence of delaminated area, the designed buckling strength of the laminated structures can be reduced when it is subjected to the compressive loading. As delamination is a major failure in the composite materials either laminates or a sandwich structure, the delamination buckling has been extensively studied in the literature. Various researches have been attempted to model and analyze the delamination buckling problem of beam or plate-type composite structures. Yin [5] studied the effects of laminated structure on delamination buckling and growth. He obtained cylindrical postbuckling solutions for an arbitrarily structured laminate applied the postbuckling solutions for a laminate with clamped ends. Chai et al. [6] conducted one-dimensional buckling analysis of single delaminated composite laminate plates. Simitses et al. [7] investigated the effect of delamination under axial loading for the twenty seven homogeneous laminated plates. Chai and Babcock [8] developed a two dimensional model of the compressive failure in delaminated laminates. Yin et al. [9] conducted the research on the ultimate axial load capacity of a delaminated

beam. Minguet et al. [10] studied the compressive failure of sandwich panels with a variety of core materials including honeycomb core. They observed three types of failure modes: core failure, debond and face-sheet fracture. Based on the test results, they developed a nonlinear model to predict these failures using appropriate failure criteria for each failure mode. An extensive experimental study was conducted by Kardomateas [11], to understand the buckling and post-buckling behavior of delaminated Kevlar/epoxy laminates. The experimental program documented the load-deflection diagrams, deformation shape in post-buckling and growth of delamination. Somer et al. [12] studied the local buckling of delaminated sandwich beams, and presented a method of continuous analysis to predict the local delamination buckling load of the face sheet of sandwich beams. Hwu and Hu [13] extended to conduct the research on the ultimate axial load capacity of a delaminated beam for the case of debonded sandwich beams. They developed formulas for buckling loads in terms of sandwich beam properties and debond length. Lim and Parsons [14] used the Rayleigh-Ritz method to analyze the buckling behavior of multiple delaminated beams. Suemasu [15] investigated the compressive buckling of composite panels with through-width; equally spaced multiple delaminations are investigated analytically and experimentally. Later, Chen [16] used a large deflection and shear deformation theory to derive the closed form expressions for the critical buckling load and post-buckling deflection of asymmetric laminates with clamped edges. Yeh and Tan [17] studied the buckling of laminated plates with elliptic delamination. Cheng et al. [18] presented

a method of continuous analysis for predicting the local delamination buckling load of the face sheet of sandwich beams. The effect of transverse normal and shear resistance from the core is accounted. The analytical procedure allowing direct determination of the buckling load by considering the entire region without separating it into regions with and without delamination is effective for this class of problem. Hwu and Hsieh [19] investigated the effect of transverse shear stress on the buckling of the delaminated composite sandwich beams. In this research, a theoretical model for the mechanical analysis of the sandwich composite plates was developed. Through this model, they obtained several analytical closed-form solutions including the solutions for the buckling loads and natural frequency. Zhang and Yu [20] analyzed delamination growth driven by the local buckling of laminate plates. Li et al. [21] presented the buckling analysis of delaminated beams based on the high-order shear deformation theory. Sekine et al. [22] investigated the buckling analysis of elliptically delaminated composite laminates by taking into account of partial closure of delamination. Yu and Hutchinson [23] analyzed a straight-sided delamination buckling with a focus on the effects of substrate compliance. Shu and Parlapalli [24] developed a one-dimensional mathematical model using Bernoulli–Euler beam theory to analyze the buckling behavior of a two-layered beam with single asymmetric delamination for simple supported and clamped boundary conditions. Mahfuz et al. [25] investigated the buckling of sandwich composites; effects of core-skin debonding and core density. In this work, a systematic approach in studying the core-skin debonds coupled with core

materials densities has been studied. Experimental, analytical and finite element studies have been conducted in this research to assess and measure the critical buckling load, deformation behavior and the failure modes under edge-wise compressive load.

2.1.2 Post-Impact Residual Strength of Composite Structures

Sandwich composite structures are susceptible to internal damage caused by low velocity impact, which can reduce the mechanical properties of the composite materials significantly. The compression after impact testing data plays an important role in composite structures design because the strength of these composites is acutely reduced whether the impact damage is visually detectable or undetectable. The estimating sensitivity of the CAI strength to low velocity impact damage has been investigated by many researchers. Dost et al. [26] found that laminate stacking sequence was critical to compression after impact strength. They concluded that the CAI strength was negatively affected when plies of the same orientation were grouped together. They also found that the symmetry of the damage through the thickness increased during these cases. The data was then examined using a sublaminate stability analysis to find the effective reduced stiffness of the impact damage zone. A stress concentration associated with the reduced stiffness was calculated and then a maximum strain failure criteria was applied to predict CAI strength. They also found that $[45/90/-45/0]_{3S}$ stacking sequence had relatively high CAI strength. Hitchen and Kemp [27] also studied the

effect of stacking sequence on impact damage of carbon/epoxy laminates. They found that 45 degree surface plies increased the energy required to initiate delamination. The initiation energy was also increased by increasing the number of dissimilar interfaces within the laminate. CAI strength decreased as the maximum delamination area increased but no relation between the two factors was determined. As well, the CAI strength did not show any trend with the surface ply orientation or the number of dissimilar interfaces. An analytical method to predict residual compressive strength was developed by Xiong et al. [28]. Their model is based on the largest sublaminate near the back surface of the specimen buckling, which is followed by the buckling of other sublaminates in the damage area. This results in a reduction in the elastic modulus at the damage area and causes the load to be redistributed to undamaged areas. This causes a stress concentration developed at the edge of the damage and reduces the compressive strength of the specimen. By using this knowledge the authors simulated the impact damage as an elliptical soft inclusion. Ishikawa and Suemasu [29] investigated the Clarification of mechanical behavior in CAI and open hole compression tests for carbon/polymer composites. Suemasu et al. [30] studied the Compressive behavior of composite laminates with different size multiple delaminations. Davies and Zhang [31] conducted research in Impact damage prediction in carbon composite structures. They described a strategy for predicting the extent of internal damage for damaged carbon fiber laminate composite structures. They found that residual strength in compression is affected much more by internal delamination

than tension structures. Soutis and Curtis [32] studied experimentally the impact and post impact compressive damage and failure of continuous carbon fiber/epoxy composites in order to predict their residual strength. They applied the fracture toughness model to predict CAI strength. Zhou and Rivera [33] investigated the effects of predictive characteristics on the residual compressive strength of 16-ply carbon/epoxy panels through the establishment of their compressive and buckling response characteristics. The possibility of delamination propagation is examined using the response characteristics on the basis of sequences.

2.1.3 Post-Impact Fatigue Behavior of Composites Structures

Structural components of machines, vehicles, and planes are frequently subjected to repeated or cyclic loading. The resulting cyclic stresses can result in a microscopic physical damage to the materials. Then, the microscopic damage can accumulate with continued cyclic loading until it develops into a crack that could lead to the failure of the material. This process of damage and failure due to cyclic loading is called fatigue. Fatigue is a dynamic phenomenon that initiates microcracks in the material and causes them to grow into large macrocracks. These cracks can lead to the catastrophic failure of the material. The Sandwich structures have a potential to be utilized in transport industries where structures are subjected to vibration or cyclic loading. The fatigue resistance and the associated failure modes under various stresses are very important to be understood. Fatigue strength of sandwich materials under different fatigue loading

including compression, tensile, and flexural stress states are important to be obtained and used when the composite structures are designed. A number of researchers have focused their studies on the fatigue behavior of composite laminates. Rosenfeld and Gause [34] studied the Compression Fatigue Behavior of Graphite/Epoxy in the Presence of Stress Raisers. They found out that tension-compression loading of graphite/epoxy laminates with load/stress ratio (R) = -1 was worst then for compression-compression loading with R = 0. However, both showed significant reductions in fatigue life when compared to tension-tension fatigue testing. Ramkumar [35] conducted an experimental work that investigated the effect of embedded delaminations on the compression fatigue behavior of quasi-isotropic T300/5208 graphite/epoxy laminates. He tested different stacking sequences of a 64-ply layup. The predominant failure mode in the test specimens was the propagation of embedded delaminations to the tab region. He considered two types of the delamination including a one dimensional delamination, located under the surface ply across the entire width, and a two dimensional circular delamination, buried one or four plies below the surface. During fatigue, the growth of an embedded delamination was monitored using diiodobutane (DIB)-enhanced radiography and S-N, half-life residual strength, and ultimate strength data were obtained. Griffin and Becht [36] carried out an experimental work to study the fatigue behavior of impact damaged BMI and thermoplastic graphite composites. Static and fatigue tests were conducted for two types of impact damaged specimens including IM7/5250-4 (bismaleimide) and IM8/HTA (thermoplastic)

composites. The results showed that the damage growth during fatigue loading was negligible for the thermoplastic, and the thermoplastic has steeper slope of the maximum stress versus fatigue cycles curve than bismaleimide. Ong et al. [37] studied the fatigue characteristics of composites after impact. The post-impact fatigue tests of AS4/APC-2 (graphite/PEEK) and T300/976 (graphite/epoxy) laminates of quasi-isotropic lay-up were conducted. Swanson et al. [38] investigated the compression Fatigue Response for Carbon Fiber with Conventional and Toughened Epoxy Matrices with Damage. The open hole compression, post-Impact compression, compression fatigue of specimens with open hole, and compression fatigue after impact response of quasi-isotropic laminates with IM7 carbon fiber and 3501-6 and 8551-7 epoxy matrices were compared in this research. They used matrices which can be considered to be a relatively brittle and a high-toughness resin, respectively. The results of impact and compression fatigue tests show that residual strengths of the toughened epoxy matrix system were approximately twice of the brittle ones, and post-impact fatigue resistance and of open hole specimens was generally improved. Mitrovic et al. [39] investigated the long-term mechanical fatigue of AS4/3501-6 graphite/epoxy quasi-isotropic laminates to determine the influence of loading parameters on impact-induced delamination growth during constant amplitude, block, and spectrum fatigue loading. They performed residual and fatigue tests on graphite/epoxy specimens. They discovered that for two-stage loading the high/low testing sequence causes more damage than the low/high. They stated

that overall delamination area alone does not represent a reliable damage parameter for residual strength. The extent of damage along the thickness is also required. The researchers also found that residual compressive strength was diminished by impact, but did not further decrease after fatigue loading. Beheshty et al. [40] observed that the effects of impact damage on carbon/epoxy (CFRP) and glass/epoxy specimens were more severe for compression-compression fatigue loading then for tension-compression loading. For tension-compression fatigue testing of CFRP, Symons and Davis [41] found that there was a slow decrease in coupon modulus as the test proceeded. They also found that the delamination area as measured by C-scan increased very little as the test proceeded. Colombo and Vergani [42] experimentally studied the effect of delamination on tensile fatigue behavior of a glass fiber reinforced composite. They performed fatigue tests to check the effect of delamination on the fatigue performance of fiberglass composite specimens, and they identified a high cycle fatigue limit for this composite. From the results, they found tensile static properties are not affected by the presence of a delamination in these specimens. However, tests revealed that the fatigue life is reduced by almost 40%. Chen et al. [43] developed non-destructive evaluation (NDE) techniques to monitor damage development during fatigue experiments in composite materials by utilizing an outstanding new ultrasonic imaging technique called acoustography. The successful combination of acoustography and a servo-hydraulic fatigue test machine has resulted in a new measurement system which can be used for the in

situ monitoring in real time of damage growth in composite specimens during long-term fatigue tests. They presented results that show damage-area growth during fatigue cycling under high compressive loads. Melin and Schon [44] studied delamination growth on a ply level with ultrasonic C-scan together with detailed measurements of the buckling shape and growth using digital speckle photography. The delamination growth and hence the damage growth is expected to be related to the fatigue life of the specimens in compressive load. They observed that the delamination growth occurs mainly in transverse direction to the load and that buckles on the backside usually have the same shape as some of the delaminations. This research showed that the buckling which takes place during the compressive part of the load cycle drives delamination growth. Gower and Shaw [45] conducted a program of experimental work designed to evaluate the applicability of static CAI and open-hole tension (OHT) procedures for the assessment of defect criticality under constant amplitude fatigue loading. They used an impact excitation technique for measurement of elastic properties after pre-defined numbers of load cycles and pulse thermography for detecting damage in coupons. The results of this study evaluated the suitability and practicality of adapting static CAI and OHT test methods for use under fatigue loading. For two different types of CFRP, Uda et al. [46] found that the delamination area was larger and the residual compressive strength was lower for the material with the lower toughness value. It was observed that the specimens with the tougher resin were less likely to fail due to propagation of delaminations during compression fatigue

testing, and more likely to fail by banding within individual laminate at a stress concentration. Kulkarni et al. [47] investigated fatigue crack growth and life predication of foam core sandwich composites under flexural loading. They found that the debond propagated slowly along the top interface and eventually kinked into the core as shear crack and then grew in unstable manner resulting in total specimen collapse. Freeman and his co-researchers [48] studied the effect of low-velocity impact on the fatigue life of composite sandwich samples consisting of two and four layer face sheet carbon fiber sandwich composite samples with foam filled honeycomb core. A drop tester was used to impact these specimens in a low velocity at three different energy levels: 10, 20, and 30J with varying masses and velocities of the impactor. Belingardi et al. [49] investigated experimentally the fatigue behavior of honeycomb sandwich beams through four-point bending tests. Two different failure mechanisms were found: the undamaged specimen failure is due to collapse occurred on compression face, while the failure of damaged specimen failure occurs due to the collapse of the honeycomb cell walls at the tip of the debonded portion. Soni et al. [50] studied the effects of low temperatures on low cycle flexural fatigue behavior of the composite sandwich beams. Bezazi et al [51] conducted the analysis of stiffness degradation and the identification of damage mechanisms during and after fatigue tests of sandwich panels with PVC foam cores. They investigated two PVC cores of similar type but with differing densities. Belouettar et al. [52] investigated static and fatigue behaviors of honeycomb sandwich composites, made of aramide fibers and aluminum cores,

through four-point bending tests. They reported and discussed damage and failure modes. Teixeira de Freitas et al. [53] investigated the fatigue behavior of the bonded and sandwich systems for strengthening orthotropic bridge decks. They performed three and four point bending fatigue tests on beams specimens representing the reinforced deck, and they found the major fatigue failure mode of the bonded system is shear failure of the adhesive layer. Nettles et al. [54] investigated and examined in-plane compressive fatigue loading after impact for sandwich composites for vehicle hardware. The results showed that the fatigue limit was about 80% of the static CAI strength, below which fatigue had no deleterious effects up to 10,000 cycles. However, the stress amplitude of about 60% of the static CAI strength was found by other studies from the literature to exist, below which fatigue had no deleterious effects up to one million cycles. Shyprykevich et al. [55] studied the guidelines needed for making analysis, testing and inspecting of Impact-damaged Composite Sandwich Structures. They presented results that shows a composite structure subjected to the repeated loading gradually loses its strength and the fatigue degradation depends on the stress amplitude and stress ratio (R). It is suggested that changes in stiffness might be an appropriate measure of fatigue damage. Hwang and Han [56] studied fatigue of composites and life prediction. They studied fatigue behavior of glass fiber reinforced epoxy composite by an analytical approach. They introduced a new concept named fatigue modulus which is defined as a slope of applied stress and resultant strain at a specific cycle. They formulated theoretical equation for

predicting fatigue life by using the fatigue modulus and its degradation rate and made attempt to find the relationship between fatigue modulus and elastic modulus by the geometric relation from stress-strain curve under the cyclic loading.

2.2 Objectives

This present research work describes the characterization of the effects of low-velocity impact damage on in-plane buckling and compression fatigue performance of new sandwich system of composite consisting of end-grain balsa wood as core and 0/90 E-glass/epoxy composites laminate as face sheets. The objective of this study is to examine the effect of damage induced by low velocity impact on the buckling behavior of sandwich composites and to experimentally assess compression-compression fatigue behavior of composite sandwich beams with impact delamination between the core and the face sheet. The two main objectives of the current research product are elaborated as follows:

The first objective is to present a combined analytical and experimental study for buckling of delaminated sandwich beams. Analytical calculations were conducted to compute critical loads by utilizing the theoretical model, and the experimental work was carried out to verify the analytical approach and solutions. The second objective is to conduct compression-compression fatigue tests for impacted and non-impacted specimens. Compressive residual strengths were obtained and the growth of delamination was monitored during fatigue.

The influence of impact damage on the failure modes and fatigue life of these sandwich beams were investigated during compression cyclic load tests. Although sandwich composites are primarily utilized for flexural loading applications, in-plane loading are not uncommon as in [51]. Rationale for us to conduct the in-plane compressive fatigue study was three-fold: (1) compressive loads lead to significant delamination near impacted zones at the core/face sheet interface with serious effects on structural integrity, (2) by studying the pure compression fatigue i.e., under in-plane loading, we will have better insight on the critical effects of damage on the sandwich composite durability. Since pure compression allows for uniform stress in the cross-section compared with gradient stress above the neutral axis in the flexural case, pure compression case provides the worst case scenario and can be used to predict the behavior of the sandwich composite more conservatively, and (3) damage development and failure mode interactions are more complex under bending loads which produce both tension and compression and their individual effects are often not separable.

The finite element analysis was performed using finite element package ABAQUS to predict the face sheet/core interface stress, and stress distribution through thickness of the undamaged composite sandwich beams.

CHAPTER THREE

BUCKLING OF DELAMINATED COMPOSITE SANDWICH BEAMS

Composite sandwich beam is commonly used in structures where strength, stiffness, and weight efficiencies are required. Debonding of the face-sheet from the core is a serious problem in sandwich beam constructions. Delamination may occur due to a variety of reasons such as low energy impact, manufacturing defects, or high stress concentration at geometric or material discontinuities. Local delamination buckling is a common failure mode in the sandwich beam structures when in-plane compressive loads are applied.

3.1 Composite Sandwich Beams

Hwu and Hsieh [19] studied the effects of delamination on the sandwich beams by developing a theoretical model for the mechanical analysis of the composite sandwich plates. There are two assumptions used in this mathematical model. The transverse shear stress distribution is assumed to be uniform across the core thickness, and the delamination supposed be free from traction provided that the delamination remains open under the axial compressive loads. All the terms containing the transverse shear stiffness have been neglected in order to get a solution satisfying with these two assumptions. This mathematical model for the buckling analysis of the composite sandwich plates was proposed by Hwu and Hu [13]. To analyze the composite sandwich beams, a corresponding one-dimensional model has also been developed based on the model of the sandwich

plate. A sandwich plate with balanced and unbalanced anisotropic composite laminated faces and ideally orthotropic honeycomb core was considered by Hwu and Hu. The basic assumptions are usually made for sandwich composites to simplify the analysis [13]:

1. The thickness of the faces are relatively much smaller than the depth of the core.

2. The transverse shear forces which can be contributed by the faces is negligible as compared with those contributed by the core and the main function of the facings is to carry loads in their own planes only.

3. The direction of the core stiffness is normal to the faces and even shear stiffness in planes is also normal to the faces.

4. The adhesive joint between the faces and the core should be strong enough to insure that any displacement in the core adjacent to the faces is reproduced in the faces, and vice versa.

Based on these assumptions, the face take almost all of the in-plane loadings and bending moments and the core takes only transverse shear and normal forces. Thus, the stress strain relationships for the orthotropic core are:

$$\sigma_x = \sigma_y = \tau_{xy} = 0, \sigma_z = E_z \varepsilon_z, \tau_{xz} = G_{xz} \gamma_{xz}, \tau_{yz} = G_{yz} \gamma_{yz} \qquad (3.1)$$

Where E_z, G_{xz} and G_{yz} are the young modulus in the z direction and the transverse shear moduli in x-z and y-z planes. In this case, the absences of three stress components lead to the strain-displacement equation and the equilibrium equation can be expressed as following:

$$\varepsilon_z = \frac{\partial w}{\partial z}, \gamma_{yz} = \frac{\partial w}{\partial y} + \frac{\partial v}{\partial z}, \gamma_{xz} = \frac{\partial w}{\partial x} + \frac{\partial u}{\partial z} \tag{3.2}$$

$$\frac{\partial \tau_{xz}}{\partial z} = 0, \frac{\partial \tau_{yz}}{\partial z} = 0, \frac{\partial \tau_{xz}}{\partial x} + \frac{\partial \tau_{yz}}{\partial y} + \frac{\partial \sigma_z}{\partial z} = 0 \tag{3.3}$$

Equation (3.3) shows that τ_{xz} and τ_{yz} are functions of x and y only and can be used to obtain σ_z:

$$\sigma_z = -z \left(\frac{\partial \tau_{xz}}{\partial x} + \frac{\partial \tau_{yz}}{\partial y} \right) + \sigma_{z0} \tag{3.4}$$

Where σ_{z0} is the value of σ_z at Z=0 and is function of x and y only. By substituting the stresses for the strains in equation (3.1) and integrating equation (3.2), three displacements can be obtained as in following relations:

$$u = \frac{z^3}{6E_z} \frac{\partial}{\partial x} \left(G_{xz} \frac{\partial \gamma_{xz}}{\partial x} + G_{yz} \frac{\partial \gamma_{yz}}{\partial y} \right) - \frac{z^2}{2E_z} \frac{\partial \sigma_{z0}}{\partial x} + z \left(\gamma_{xz} + \frac{\partial w_0}{\partial x} \right) + u_0 \tag{3.5}$$

$$v = \frac{z^3}{6E_z} \frac{\partial}{\partial y} \left(G_{xz} \frac{\partial \gamma_{xz}}{\partial x} + G_{yz} \frac{\partial \gamma_{yz}}{\partial y} \right) - \frac{z^2}{2E_z} \frac{\partial \sigma_{z0}}{\partial y} + z \left(\gamma_{yz} + \frac{\partial w_0}{\partial y} \right) + v_0 \tag{3.6}$$

$$w = \frac{-z^2}{2E_z} \frac{\partial}{\partial x} \left(G_{xz} \frac{\partial \gamma_{xz}}{\partial x} + G_{yz} \frac{\partial \gamma_{yz}}{\partial y} \right) + z \frac{\sigma_{z0}}{E_z} + w_0 \tag{3.7}$$

Where u_0, v_0 and w_0 are the displacements of the plane at z = 0, and σ_{z0}, γ_{xz}, and γ_{yz} are functions of x and y. the assumption here is that the core normal transverse stiffness E_z is infinity large due to the negligibility of the transverse normal strains for the sandwich composite structure where the honeycomb is used to be the core. Based on this assumption, equations (3.5), (3.6), and (3.7) expressed the core displacements can be reduced as following:

$$u = u_0 + z\left(\gamma_{xz} - \frac{\partial w_0}{\partial x}\right) \tag{3.8}$$

$$v = v_0 + z\left(\gamma_{yz} - \frac{\partial w_0}{\partial y}\right) \tag{3.9}$$

$$w = w_0 \tag{3.10}$$

Which the model is usually given by the shear deformation plate theory.

Since the delamination buckling and post buckling are the main concern on this study, finite deformation should be considered and included. If the deformations are considered are functions of x, y, and z (the position of points in the unstrained configurations), the lagrangian strains ε_x and ε_y and γ_{xy} can be evaluated with the aid of equations (3.8), (3.9), and (3.10) as:

$$\varepsilon_x = \frac{\partial u}{\partial x} + \frac{1}{2}\left(\frac{\partial w_0}{\partial x}\right)^2 = \varepsilon_{x_0} + z\kappa_x \tag{3.11}$$

$$\varepsilon_y = \frac{\partial v}{\partial y} + \frac{1}{2}\left(\frac{\partial w_0}{\partial y}\right)^2 = \varepsilon_{y_0} + z\kappa_y \tag{3.12}$$

$$\gamma_{xy} = \frac{\partial u}{\partial y} + \frac{\partial v}{\partial x} + \frac{\partial w}{\partial x}\frac{\partial w}{\partial x} = \gamma_{xy_0} + z\kappa_{xy} \tag{3.13}$$

Where

$$\varepsilon_{x_0} = \frac{\partial u_0}{\partial x} + \frac{1}{2}\left(\frac{\partial w_0}{\partial x}\right)^2 \tag{3.14}$$

$$\varepsilon_{y_0} = \frac{\partial v_0}{\partial y} + \frac{1}{2}\left(\frac{\partial w_0}{\partial y}\right)^2 \tag{3.15}$$

$$\gamma_{xy_0} = \frac{\partial u_0}{\partial y} + \frac{\partial v_0}{\partial x} + \frac{\partial w_0}{\partial x} \frac{\partial w_0}{\partial x} \tag{3.16}$$

$$\kappa_x = \frac{\partial}{\partial x}\left(\gamma_{xz} - \frac{\partial w_0}{\partial x}\right) \tag{3.17}$$

$$\kappa_y = \frac{\partial}{\partial y}\left(\gamma_{yz} - \frac{\partial w_0}{\partial y}\right) \tag{3.18}$$

$$\kappa_{xy} = \frac{\partial}{\partial y}\left(\gamma_{xz} - \frac{\partial w_0}{\partial x}\right) + \frac{\partial}{\partial x}\left(\gamma_{yz} - \frac{\partial w_0}{\partial y}\right) \tag{3.19}$$

As the faces are firmly united to the core, the displacements in the core bonded to the faces are duplicated precisely in the faces. Thus, the displacements of the faces adjacent to the core can be calculated and obtained by substituting $z = \pm c/2$ into equations (3.8), (3.9), and (3.10) where positive and negative signs, respectively, for lower and upper faces. Consequently, it is natural to assume the displacements of the faces have the form as those of the core described in equations (3.8), (3.9), and (3.10). It should be notated that the plane of $z = 0$ for the face sheet displacements is still be the mid-plane of the core, not mid-plane of the face. Furthermore, the transverse shear deformation is included in this expression, even though shear forces can be neglected comparted to those contributed by the core since the thickness of the faces are relatively thinner than the core thickness.

With the same form as the displacements of the core given in equations (3.8), (3.9), and (3.10), the resulting forces and moments contributed by the face can be defined by the way which is similar to the classical lamination theory (CLT).

The coordinate system, resultant forces and moments for laminated plate is shown in Fig. 3.1. The geometry of the laminated plate and ply numbering is also shown in Fig. 3.2
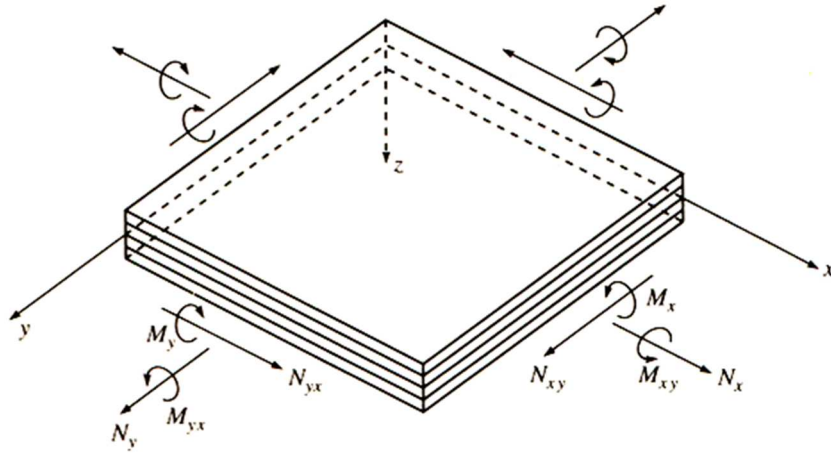
Fig. 3.1. Coordinate system and stress resultant for laminated plate [4]
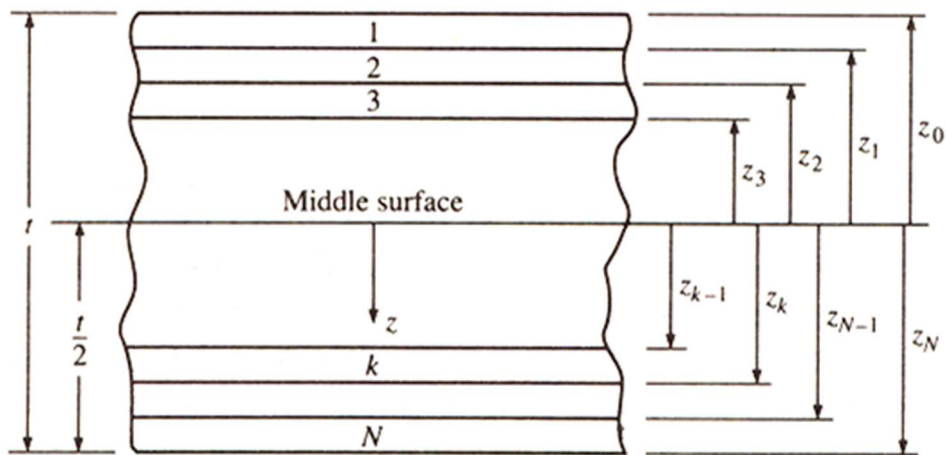
Fig. 3.2. Laminated plate geometry and ply numbering system [4]

The resultant forces, moments, and the complete set of equations can be expressed in matrix form as:

$$
\begin{Bmatrix} N_x \\ N_y \\ N_{xy} \\ M_x \\ M_y \\ M_{xy} \end{Bmatrix} = \begin{bmatrix} A_{11} & A_{12} & A_{16} & B_{11} & B_{12} & B_{16} \\ A_{12} & A_{22} & A_{26} & B_{12} & B_{22} & B_{26} \\ A_{16} & A_{26} & A_{66} & B_{16} & B_{26} & B_{66} \\ B_{11} & B_{12} & B_{16} & D_{11} & D_{12} & D_{16} \\ B_{12} & B_{22} & B_{26} & D_{12} & D_{22} & D_{26} \\ B_{16} & B_{26} & B_{66} & D_{16} & D_{26} & D_{66} \end{bmatrix} \begin{Bmatrix} \varepsilon_{x0} \\ \varepsilon_{y0} \\ \gamma_{xy0} \\ \kappa_x \\ \kappa_y \\ \kappa_{xy} \end{Bmatrix}
\tag{3.20}
$$

Or in partitioned form as:

$$
\begin{Bmatrix} N \\ -- \\ M \end{Bmatrix} = \begin{bmatrix} A & \vdots & B \\ --&+&-- \\ B & \vdots & D \end{bmatrix} \begin{Bmatrix} \varepsilon_0 \\ -- \\ \kappa \end{Bmatrix}
\tag{3.21}
$$

Where:

$$
A_{ij} = \int_{-t/2}^{t/2} \left(\overline{Q}_{ij} \right)_k dz = \sum_{k=1}^{N} \left(\overline{Q}_{ij} \right)_k (z_k - z_{k-1})
\tag{3.22}
$$

$$
B_{ij} = \int_{-t/2}^{t/2} \left(\overline{Q}_{ij} \right)_k z \, dz = \frac{1}{2} \sum_{k=1}^{N} \left(\overline{Q}_{ij} \right)_k (z_k^2 - z_{k-1}^2)
\tag{3.23}
$$

$$
D_{ij} = \int_{-t/2}^{t/2} \left(\overline{Q}_{ij} \right)_k z^2 \, dz = \frac{1}{3} \sum_{k=1}^{N} \left(\overline{Q}_{ij} \right)_k (z_k^3 - z_{k-1}^3)
\tag{3.24}
$$

A_{11}, B_{11}, D_{11} and S are called, respectively, the extensional, coupling, bending, and transverse shear stiffness of the composite sandwich plate. Unlike the classical lamination theory in which A_{ij} (extensional stiffness), B_{ij} (coupling stiffness) and D_{ij} (bending stiffness) are calculated based on the coordinate where z = 0 is the middle surface of the laminate (Fig. 3.2), but here the plane z = 0 is located on the mid-surface of the core. Hence the following can be concluded that B_{ij} = 0 for

symmetric laminates and that $A_{16}, A_{26}, D_{16},$ and D_{26} = 0 for antisymmetric laminates may not be valid in each face but may be valid when overall sandwich is symmetric or antisymmetric.

As transverse shear forces contributed by the faces are negligible, the transverse shear forces contributed by the core can be expressed as:

$$\begin{Bmatrix} Q_X \\ Q_Y \end{Bmatrix} = c \begin{Bmatrix} G_{xz} \ \gamma_{xz} \\ G_{yz} \ \gamma_{yz} \end{Bmatrix} \tag{3.25}$$

The expression shown in equation (3.25) may represent the total transverse shear force the sandwich plates.

The equilibrium equations for the buckled sandwich plate expressed by the resultant forces are:

$$\frac{\partial N_x}{\partial x} + \frac{\partial N_{xy}}{\partial y} = 0 \tag{3.26}$$

$$\frac{\partial N_{xy}}{\partial x} + \frac{\partial N_y}{\partial y} = 0 \tag{3.27}$$

$$\frac{\partial Q_x}{\partial x} + \frac{\partial Q_Y}{\partial y} + \frac{\partial v}{\partial y} + N_x \frac{\partial^2 w}{\partial x^2} + 2N_{xy} \frac{\partial^2 w}{\partial x \partial y} + N_y \frac{\partial^2 w}{\partial y^2} = 0 \tag{3.28}$$

$$\frac{\partial M_x}{\partial x} + \frac{\partial M_{xy}}{\partial y} = Q_x \tag{3.29}$$

$$\frac{\partial M_{xy}}{\partial x} + \frac{\partial M_y}{\partial y} = Q_y \tag{3.30}$$

By using equations (3.14-3.25), the five equilibrium equations (3.26-3.30) for the composite sandwich plate can be written in terms of five unknown: $u_0, v_0, w_0,$

γ_{xz}, and γ_{yz}. The five equations can be further reduced to three equations for one dimensional problems, and can be expressed as:

$$\frac{\partial N_x}{\partial x} = 0 \tag{3.31}$$

$$N_X \frac{d^2 w}{dx^2} + c G_{xz} \frac{d\gamma_{xy}}{dx} = 0 \tag{3.32}$$

$$B_{11} \frac{d}{dx} \left[\frac{du_0}{dx} + \frac{1}{2} \left(\frac{\partial w_0}{\partial x} \right)^2 \right] + D_{11} \frac{d^2}{dx^2} \left(\gamma_{xz} - \frac{dw}{dx} \right) = c G_{xz} \gamma_{xz} \tag{3.33}$$

Where N_x is given by:

$$N_x = A_{11} \left[\frac{du_0}{dx} + \frac{1}{2} \left(\frac{\partial w_0}{\partial x} \right)^2 \right] + B_{11} \frac{d}{dx} \left(\gamma_{xz} - \frac{dw}{dx} \right) \tag{3.34}$$

Equation (3.30) reveals that N_X is constant through the plate and equal to the compressive axial load (P) applied at the ends.

$$N_X = -P \tag{3.35}$$

By substituting equation (3.35) into (3.32) and (3.34), we have:

$$\frac{d\gamma_{xz}}{dx} = \frac{P}{S} \frac{d^2 w}{dx^2} \tag{3.36}$$

$$\frac{du_0}{dx} = -\frac{P}{A_{11}} - \frac{1}{2} \left(\frac{\partial w_0}{\partial x} \right)^2 + \frac{B_{11}}{A_{11}} \left(1 - \frac{P}{S} \right) \frac{d^2 w}{dx^2} \tag{3.37}$$

Where $S = C G_{XZ}$ represents transverse shear stress stiffness. For one dimensional problem, the governing equation for buckled sandwich beam can also be reduced from the governing equations for the buckled plate, and can be obtained by

substituting equations (3.36) and (3.37) into (3.33), and expressed by only one

parameter w (transverse shear deflection) :

$$\frac{d^2w}{dx^2} + \lambda^2 w = c_1 x + c_2 \tag{3.38}$$

Where λ^2 is expressed as:

$$\lambda^2 = \frac{P}{\left(D_{11} - B_{11}^2 / A_{11}\right)\left(1 - P/S\right)} \tag{3.39}$$

The compressive axial load (P) is applied at the ends of the beam and x is the

longitudinal coordinate along the beam. c_1 and c_2 are the integration constants

which will be determined by the boundary conditions. The stiffness A_{11}, B_{11} and

D_{11} are contributed by the faces of the sandwiches, whereas the shear stiffness S

is mostly contributed by the core. The formulas for calculating A_{11}, B_{11} and D_{11} are

the same as those given in the CLT for laminated plate and the difference is only

that the plane $z = 0$ is located on the mid-surface of the entire sandwich structure

[4]. The transverse deflection w is determined by the governing equation (3.38)

and the boundary conditions set for the problems, the transverse shear strain γ_{xz}

the horizontal displacement u, the transverse shear force Q_X and the bending

moment M_x can then be calculated by the following relations:

$$\gamma_{xz} = \frac{P}{S}\left(\frac{dw}{dx} - \frac{c_1}{\lambda^2}\right) \tag{3.40}$$

$$u = -APx - \frac{1}{2}\int\left(\frac{dw}{dx}\right)^2 dx + (B-z)\left(1 - \frac{P}{S}\right)\frac{dw}{dx} - \frac{Pc_1}{S\lambda^2}z + const \tag{3.41}$$

$$Q_X = S\,\gamma_{xz} = P\left(\frac{dw}{dx} - \frac{c_1}{\lambda^2}\right) \tag{3.42}$$

$$M_x = P\left(w - \frac{c_1\,x + c_2}{\lambda^2} + B\right) \tag{3.43}$$

Where A and B are given as:

$$A = \frac{1}{A_{11}}, B = {B_{11}}/{A_{11}} \tag{3.44}$$

3.2 Analytical Sandwich Beam Model

A buckling model for delaminated sandwich composites by Hwu and Hsieh [19] was found to predict satisfactory results for specimens failing in a delamination buckling mode. In this model, a composite sandwich beam with delamination was considered. The delamination lies in the middle of the sandwich beam between the upper face and core. The beam has a constant width along its length, and is subjected to compressive axial load P at the clamped ends $x = \pm l$. The interface crack extended over an interval $-a \leq x \leq a$, and runs across the whole width of the beam as shown in Figure 3.3. When the axial compressive load reaches to the critical value, the delaminated sandwich beam starts to buckle. The entire delaminated sandwich beam is divided into three regions which are shown in Fig. 3.3 to analyze the beam. Region 1 and region 2 are considered as sandwich

beams, and a laminate beam is represented by region 3. When the governing equation is applied for these three regions, the term containing S vanish for regions 2 and 3 since $\tau_{xz} = 0$ $(\gamma_{xz} = 0)$ along the crack surfaces provided that the crack remains completely open.
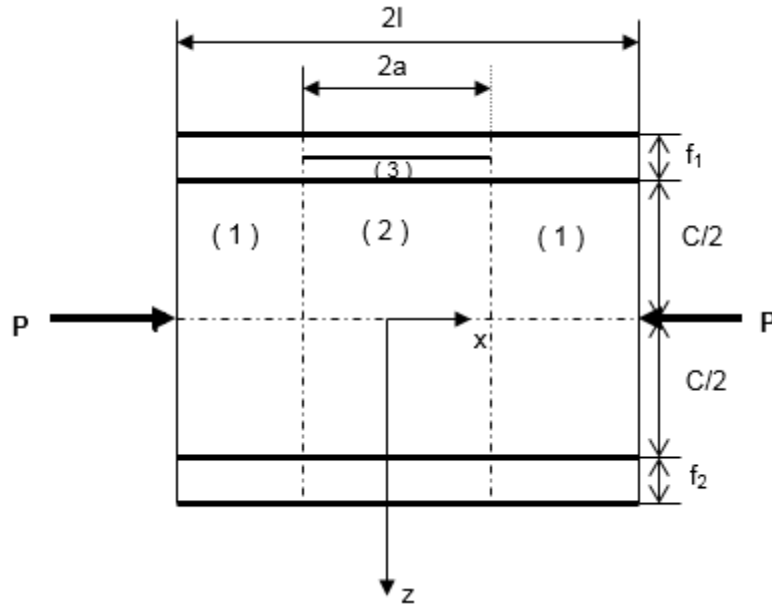
Fig. 3.3. Delaminated composite sandwich beam [19]

The shear stress is assumed to be uniform across the thickness of the core in this mathematical model, and thus the vanished shear stress along the delamination surface will lead to vanish of the shear stress for the entire core under the interface crack. In addition, shear resistance of region 2 is neglected. The solution obtained by using these assumptions may be resulted a near-zero buckling load. The zero transverse shear stress leads to zero strain shear strain as a result of the proportional relationship between them. Therefore, the zero shear deformation

along the delamination surface may lead to conventional Euler beam assumption for regions 2 and 3, and thus the shear resistance of these two regions is infinite. To determine the critical buckling load P_{cr}, the analytical solution of the governing equation under these assumptions has been found as following:

$$P_{cr} = (D_2 + D_3 - D_1) \left[\frac{a}{\bar{\lambda}_1 \tan \bar{\lambda}_1 (l-a)} + \frac{ka}{\bar{\lambda}_2 \tan \bar{\lambda}_2 \, a} + \frac{(1-a)k}{\bar{\lambda}_3 \tan \bar{\lambda}_3 \, a} \right]^{-1} \quad (3.45)$$

Where:

$$\bar{\lambda}_1^{\,2} = \frac{P_{cr}}{D_{11}\left(1- {P_{cr}}/{S}\right)} \,, \bar{\lambda}_2^{\,2} = \frac{kP_{cr}}{D_2} \,, \bar{\lambda}_3^{\,2} = \frac{(1-k)P_{cr}}{D_3} \quad (3.46)$$

$$A_i = \frac{1}{(A_{11})_i} \,, B_i = \left(\frac{B_{11}}{A_{11}}\right), D_i = \left(D_{11} - \frac{B_{11}^2}{A_{11}}\right), i = 1, 2, 3 \quad (3.47)$$

$$k = A_3/(A_2 + A_3) \,, S = cG_{xz} \quad (3.48)$$

Where:

c is core thickness and G_{xz} is the transverse shear modulus in $x - z$ plane. The formula calculating S value is based on the assumption that the transverse shear forces contributed by the faces are negligible as compared with those contributed by the core. Moreover, the transverse shear stress distribution is uniform across the thickness of the core. During the calculations of the buckling load by utilizing formula (3.45), Hwu and Hsieh [19] monitored that the solutions were usually obtained from the conditions:

$tan\,\bar{\lambda}_1(l-a)=0$, or $tan\,\bar{\lambda}_2\,a=0$, or $tan\,\bar{\lambda}_3\,a=0$, and these conditions correspond

to the following solutions:

$$P_{cr} = \frac{D_1\pi^2 / (l-a)^2}{1+ D_1\pi^2 / S_1 (l-a)^2} \qquad (3.49)$$

$$P_{cr} = \frac{D_2\pi^2/a^2}{k\,(1+ D_2\pi^2 / S_2 a^2)} \qquad (3.50)$$

$$P_{cr} = \frac{D_3\pi^2}{(1-k)a^2} \qquad (3.51)$$

Where:

$$S_1 = cG_{xz}, S_2 = \infty \qquad (3.52)$$

Then, the critical buckling load (P_{cr}) is calculated from equations (3.49), (3.50),

and (3.51), and the lowest value of P_{cr} can be used in design calculations.

CHAPTER FOUR

MATERIALS AND SPECIMENS

4.1 Material Description

Sandwich materials were manufactured with glass fiber laminates as face sheets and with end-grain balsa wood as core. The face sheet material used for composite sandwich panels is laminates of E-glass fibers in an epoxy (Epon 202) matrix. Each layer of the prepreg is a cross-ply of two plies stitched that were oriented to 0° and 90° (thickness = 0.45 mm). E-glass/epoxy (202) prepreg and fully cured laminate is shown in Fig. 4.1. The end-grain balsa wood was used with a density of 96 ± 5 kg/m^3 and a thickness of 6.35 mm. The sandwich panel with end-grain balsa wood, which has the grain oriented along the thickness of the sheet as shown in Fig. 4.2 is represented schematically as shown in Fig. 4.3.

(a) E-glass/ Epoxy Prepreg   (b) Fully Cured Laminate

Fig. 4.1. Prepreg material and fully cured laminate

Fig. 4.2. End-grain balsa wood
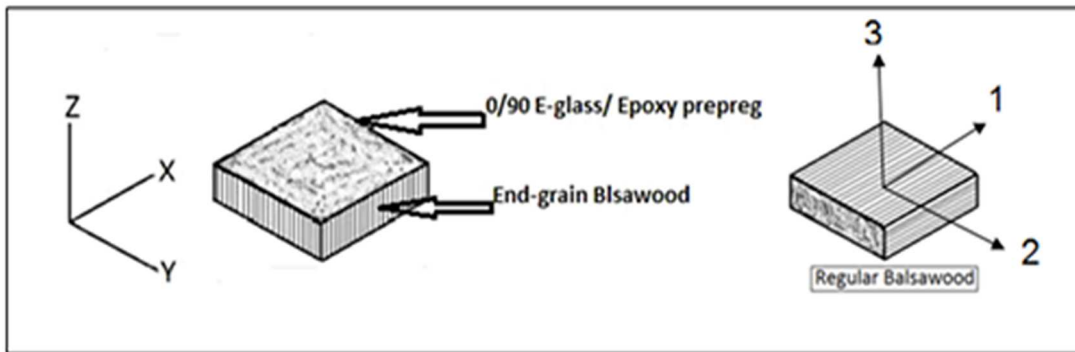
Fig. 4.3. Schematic representation of composite sandwich panel and its grain direction

Analytical models and finite element analysis require all the basic properties of materials constructed the composite sandwich structure and their behavior under various loading conditions. Hence, preliminary tests including tensile, compression, and shear were conducted on both core and face sheet materials in different directions to calculate the properties under these tests. The mechanical properties of the facing and core sandwich structures referred to material directions (L, T, T) or (1, 2, 3) are represented in Tables 4.1 and 4.2 respectively.

Table 4.1. Material properties of 0°/90°E-glass/epoxy laminate

	E-glass/epoxy laminate
Density (Kg/m^3)	1926.3
Tensile modulus,E_1,E_2,E_3 (GPa)	19.88, 19.88, 12.59
Compressive Modulus (In-plane), E_1,E_2 (Gpa)	7.42, 7.42
Shear modulus,G_{12},G_{23},G_{31} (GPa)	4.04, 3.37, 3.37
Poisson's ratio, v_{12} ,v_{23}, v_{31}	0.11, 0.18, 0.18
Longitudinal and transverse compressive strength (GPa)	0.288, 0.288
Longitudinal and transverse tensile strength (GPa)	0.545 , 0.545
Shear strength T_{12}, T_{23}, T_{13} (GPa)	0.031, 0.072, 0.072

Table 4.2. Material properties of balsa wood core

	Balsa wood core
Density (Kg/m^3)	96 ± 5
Longitudinal tensile modulus E_1 (MPa)	1683.8
Transverse tensile modulus E_2 (MPa)	54
Longitudinal compressive modulus E_1 (MPa)	460
Transverse compressive modulus E_2 (MPa)	23.5
Longitudinal shear modulus,G_{12} (MPa)	72.85
Transverse shear modulus G_{23} (MPa)	12.5
Poisson's ratio, v_{12}, v_{23}, v_{31}	0.007, 0.479, 007
Longitudinal tensile strength (MPa)	10.12
Transverse tensile strength (MPa)	0.82
Longitudinal compressive strength (MPa)	8.05
Perpendicular compressive strength (MPa)	0.707
Longitudinal shear strength (MPa)	1.35
Transverse shear strength (MPa)	1.35

4.2 Material Fabrication

These sandwich panels were fabricated by utilizing end-grain balsa wood. The dimension of the composite sandwich panel was 305 mm (length) X 305 mm (width) with 7.25 ± 0.15mm thickness, consisting of one layer of 0/90 E-glass/epoxy prepreg, layered as skin on both sides of the end-grain balsa wood core. The panel was cured in the vacuum press mold to get good adhesion at 135°C for 20 min at 344.7 kPa pressure applied on the laminate. Then, the panel was finally post-cured in convection oven at 80°C for 5 hours. The face sheet was bonded directly to the core, thus there was no need to use any adhesive between the 0/90 E-glass/epoxy prepreg and the end-grain balsa wood. A vacuum press machine, post curing oven, and fully cured sandwich panel are shown in Fig. 4.4.
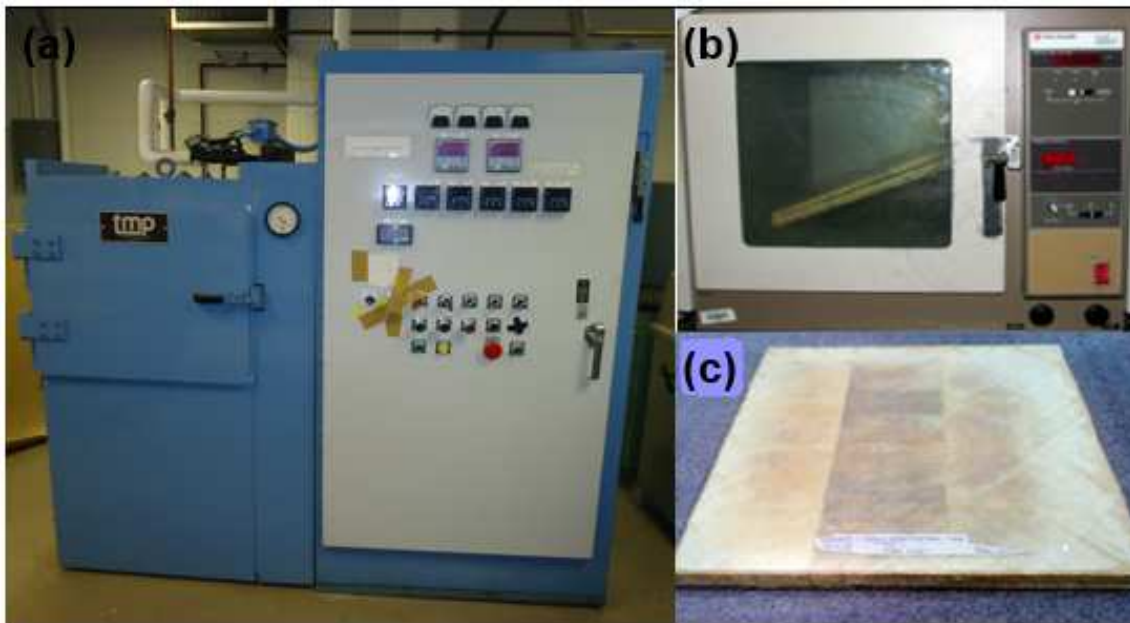
Fig. 4.4. (a) Curing machine; (b) post curing oven; (c) Fully cured composite sandwich panel.

4.3 Manufacturing of Test Specimens and Dimensions

Composite Sandwich panels were used to extract rectangular prism specimens of 25.4x7.25 mm^2 a cross-sectional area and 152.4 mm length. These specimens were cut by using a band saw as shown in Fig. 4.5 and the dimensions of the sandwich beam (SB) are listed in Table 4.3. These specimens were machined for impact and subsequent static compression and compression fatigue tests. The tests described in the following sections required different number of specimens. The dimensions and number of specimens for each test are summarized in Table 4.4.
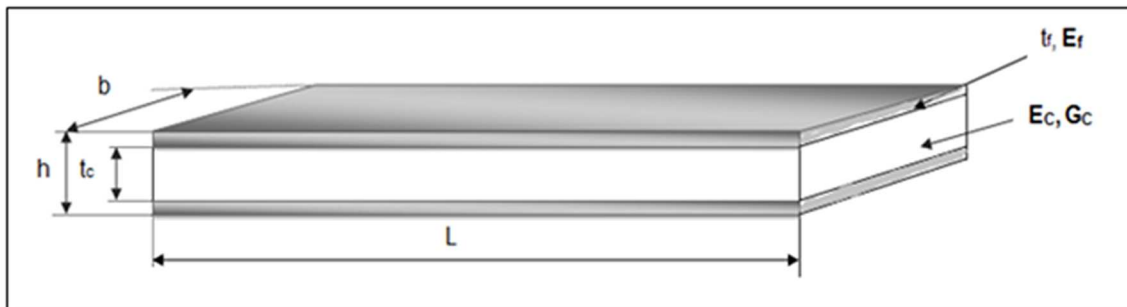
Fig. 4.5. Sketch of the specimen dimensions

Table 4.3. Specimen dimensions

L (mm)	b (mm)	t_c (mm)	t_f (mm)	h (mm)
152.4	25.4	6.35	0.45	7.25

Table 4.4. Test matrix for mechanical tests and specimen dimensions

Test	Composite Structure	Impact Energy (J)	Length (mm)	Width (mm)	Thickness (mm)	Number of Specimens
Impact test	SB	8.8	152.4	25.4	7.25	24
Compression Static test	Undamaged SB	-	152.4	25.4	7.25	12
Compression Static test	Damaged SB	8.8	152.4	25.4	7.25	12
Compression Fatigue test	Undamaged SB	-	152.4	25.4	7.25	12
Compression Fatigue test	Damaged SB	8.8	152.4	25.4	7.25	12

CHAPTER FIVE

EXPERIMENTAL WORK AND FINITE ELEMENT ANALYSIS

5.1 Experimental Work

5.1.1 Impact Test

Initial impact tests with different energies were conducted to produce impact damage for subsequent fatigue loading. The purpose of these initial tests is to find the existence of the threshold energy that causes impact damage which can be visually detected for this class of sandwich composites. Impact tests were carried out using a conventional drop weight tower with an impactor having 0.454 Kg weight and a 25.4 mm diameter hemispherical-nosed weight falling through a height of 2 m to strike each specimen centrally for an energy of 8.8 J. A total of 24 specimens were impacted in this research work and impact fixture was utilized to provide the necessary support for the specimens during impact. The specimen was supported along the long sides and clamped in gripping zones of the specimen's short sides. To prevent secondary impact, the impactor was caught manually using a cord on the rebound after impact. The test matrix for the impact test is tabulated in Table 5.1

Table 5.1. Test matrix for impact test

Type of Test	Composite Structure	Number of Samples were tested	Impact Energy (J)	Sample Dimensions (mm)
Impact Test	Composite sandwich beam	24	8.8	152.4 ×25.4×7.25

5.1.1.1 Damage Inspection

The small damage originating at the impact site was visible on the top face sheet for all of composite sandwich beams at this impact energy level. For all specimens, the damage would appear on both sides including the impact and the back sides. The length and area of the delamination was utilized to evaluate the impact response of composite sandwich beams. Therefore, precise methods should be used to estimate the size of this interface damage and here image j software was utilized to measure the damage size after taking at least two pictures of each damaged area by using a digital camera. The damage in our specimens was inspected visually, and the appearance of delamination was clear. The end-grain balsa wood core facilitates development of this delamination well. To evaluate the impact response for this class of composite sandwich beams, the damage area induced by the impact load was captured by a digital camera and then measured by image J software.

5.1.2 Compression Static Test

Compression static tests were conducted on a 200 KN MTS servo-hydraulic test machine. Compression testing of composite sandwich beams was performed in accordance with the ASTM standard method, which is D6641, the combined loading compression (CLC) test. The CLC fixture involves a combination of direct compression on the ends of an untabbed specimen and shear transfer through side loading to produce pure compression within the gage length (25 mm) in the

middle of the specimen. The setup of the compression test including CLC fixture and MTS test machine is shown in Fig. 5.1. Each specimen was compressed between two platens and loaded at a constant displacement rate of 0.05 mm/min while load and displacement were recorded using PC at every one-tenth second. Compression static tests were carried out for twelve undamaged and twelve damaged sandwich beams as summarized in Table 5.2.
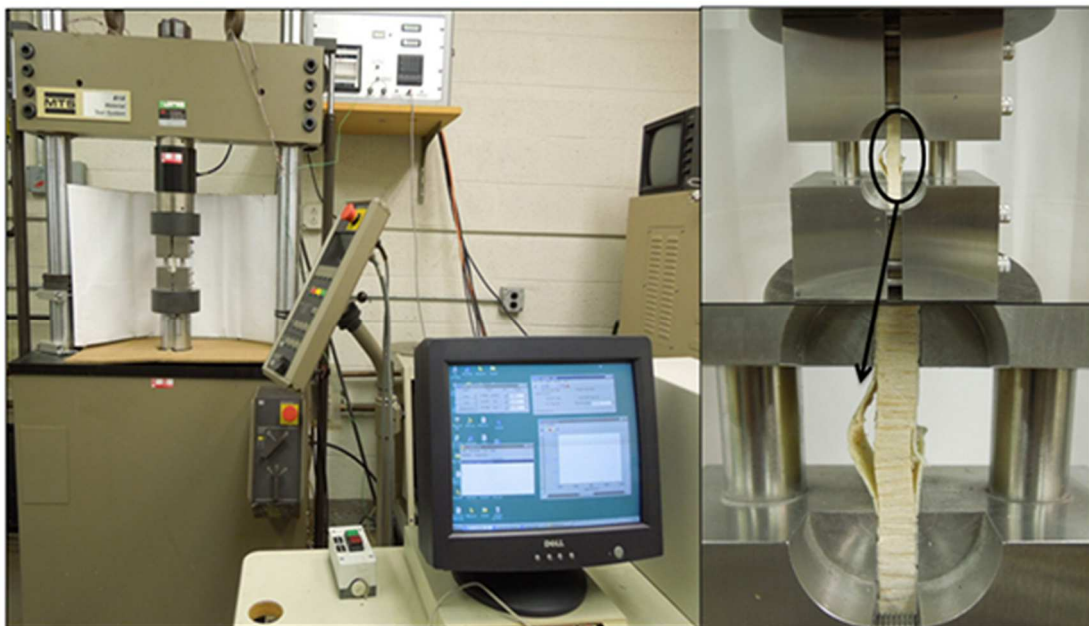
Fig. 5.1. Test setup for compression static tests

Table 5.2. Test matrix for compression static test

Type of Test	Composite Structure	Number of Samples were tested	Impact Energy (J)	Sample Dimensions (mm)
Static Compression	sandwich beam	12	Undamaged	152.4 ×25.4×7.25
Static Compression	sandwich beam	12	8.8	152.4 ×25.4×7.25

5.1.2.1 Experimental Evaluations of Critical Buckling Load (P_{cr})

Quasi-static compression tests were performed in displacement control mode for delaminated composite sandwich beams to evaluate P_{cr} experimentally. These tests were conducted by utilizing the same fixture and MTS machine which were used in the previous compression tests. The typical local buckling of a sandwich beam is shown in Fig. 5.2. Load, displacement and time data were recorded for every 0.1s by the computerized controlled machine. Pictures were captured and Videos were recorded during the compression tests. It is observed in these videos, the delaminated sandwich beam starts to buckle when the axial compressive load reaches P_{cr}. Later the videos were analyzed for critical points time of P_{cr} and were correlated with time from the experimental data.
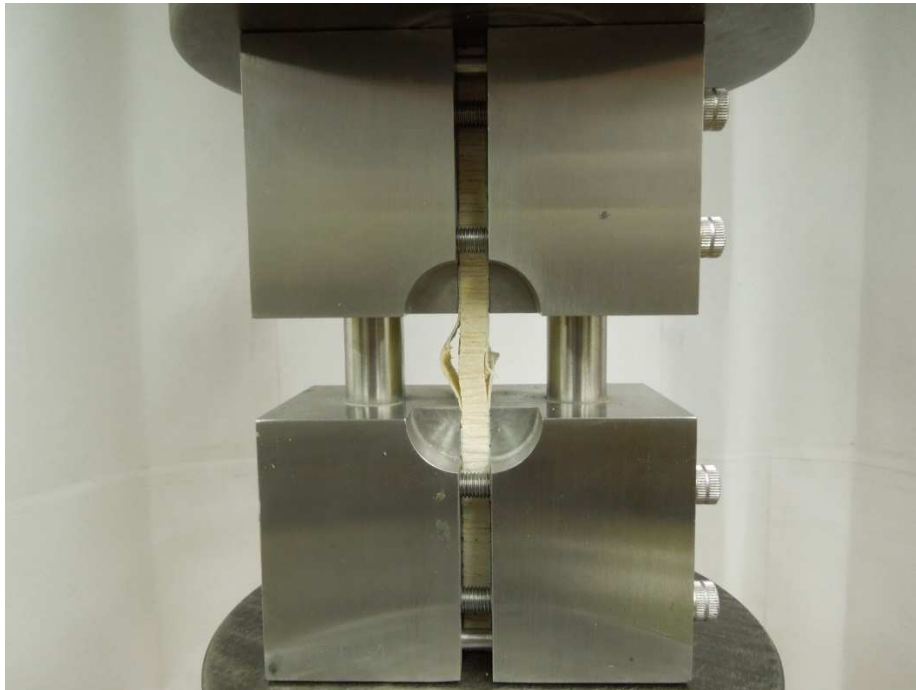
Fig. 5.2. Typical buckling of a sandwich beam

5.1.3 Compression-Compression Fatigue Test

Compression–Compression constant amplitude fatigue tests were performed to determine the influence of different loading parameters on impact-induced damage growth. The tests were conducted on a MTS testing machine with load capacity of 100KN (see Fig. 5.3) under ambient laboratory conditions at a frequency of 5 Hz and stress ratio (R) of R = 10 which was kept constant during all fatigue tests. All compression fatigue tests were under load controlled mode, and an extensometer was used to obtain strain from the beam. By using the ultimate compressive and residual strength data for undamaged and damaged sandwich beams from compression static tests, the maximum compressive load per cycle was determined at different load levels, which is defined from the following relationship:

$$r = \frac{P_{min}}{P_{ul}} \qquad (5.1)$$

Where:

P_{min} = The maximum compressive load applied per fatigue cycle

P_{ul} = The Ultimate compressive load during compression static loading

The maximum compressive load (P_{min}) level at which fatigue tests were conducted on both impacted and non-impacted composite sandwich beams, was found to be r = 0.7.During the compression-compression fatigue test, the value of R is determined from the following relationship:

$$R = \frac{\sigma_{min}}{\sigma_{max}} \qquad (5.2)$$

Where σ_{min} is the maximum compressive stress and σ_{max} is the minimum compressive stress. The maximum compressive stress (σ_{min}) of the cyclic loading was chosen to be 40% to 70% of the ultimate compressive static strength (σ_{ul}) for damaged and undamaged composite sandwich beams. Four different load levels (σ_{min}/σ_{ul}) in the range of 0.4 to 0.7 were chosen for both impacted and non-impacted sandwich beams and three specimens were tested for each stress level. Load and displacement data collected using a PC based acquisition system are obtained from the machine, which are converted into stress-strain curves. By using these data, the hysteresis loop of applied stress vs. strain in specific fatigue cycle was plot to determine the stiffness during that cycle. Typical compression cyclic load is shown in Fig. 5.4 Delamination growth in fatigue tests was monitored using a Gaertner 1601-A horizontal microscope with dimension scale in the optical eyepiece as shown in Fig. 5.3. The test matrix for compression-compression fatigue tests including the dimensions and number of specimens for each test is tabulated in Table 5.3.
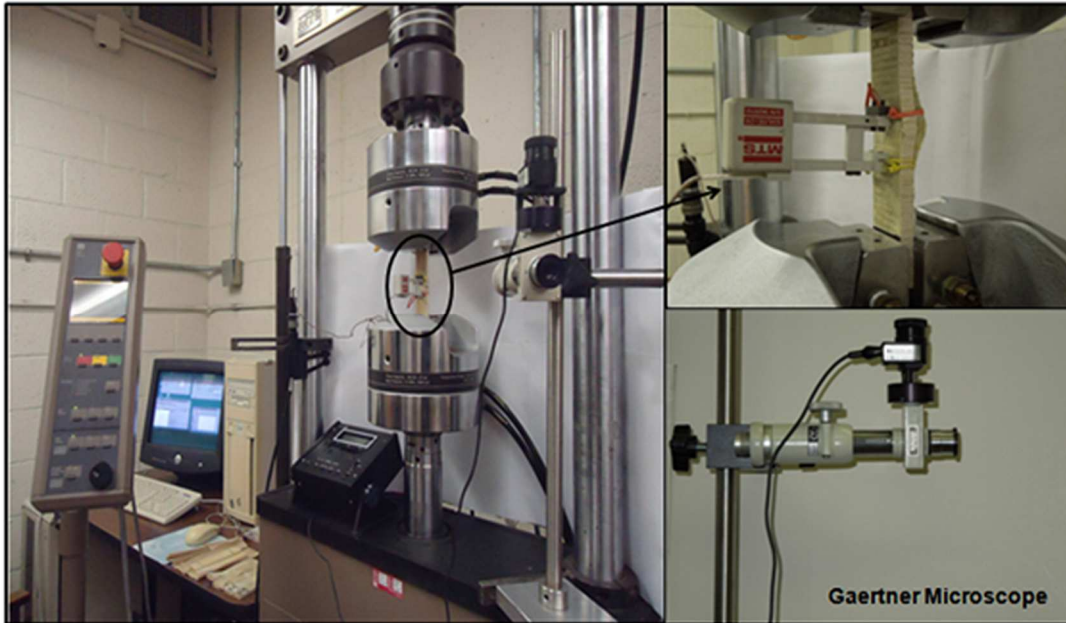
Fig. 5.3. Compression fatigue test machine, test set up for fatigue tests and Gaertner microscope
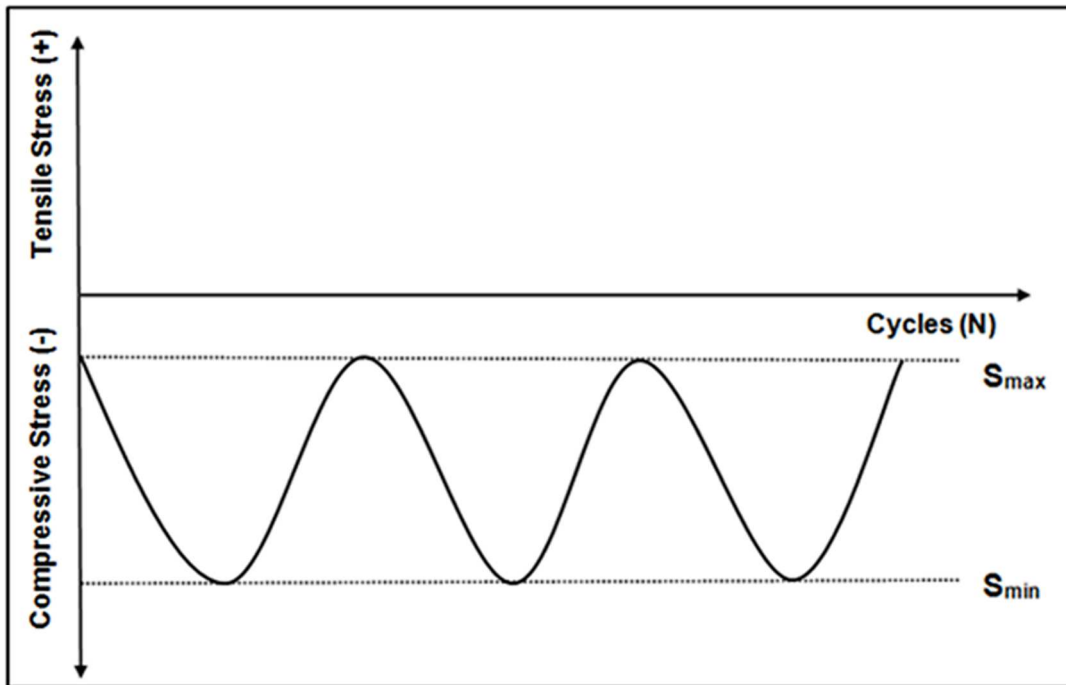
Fig. 5.4. Typical compression-compression cyclic load

Table 5.3. Test matrix for compression-compression fatigue test

Type of Test	Composite Structure	Number of Samples were tested		Impact Energy (J)	Sample Dimensions (mm)
Compression-Compression Fatigue	Composite sandwich beam	Load level (r) 0.4 o.5 0.6 0.7	Number of Samples 3 3 3 3	Undamaged	152.4 ×25.4×7.25
Compression-Compression Fatigue	Composite sandwich beam	Load level (r) 0.4 o.5 0.6 0.7	Number of Samples 3 3 3 3	8.8	152.4 ×25.4×7.25

5.2 Finite Element Analysis

In this part of this research work, the finite element analysis (FEA) was used to estimate the in-plane normal compressive stress distribution and the interfacial stress of an undamaged composite sandwich beam subjected to in-plane compressive load. As facing and core stresses of undamaged sandwich beams were determined experimentally and analytically, the face sheet/core interface stress is complex to be obtained by using the same approaches.

The static FEA was performed to predict the interfacial stress and investigate the stress distribution along the thickness of the undamaged sandwich beam. For the static FEA, HyperMesh V 11.0 used as a pre-processor and ABAQUS/Standard 6.11 was used as a solver. HyperView/HyperMesh v 11.0 was utilized as a post-processor to process the results from ABAQUS analysis.

5.2.1 Preprocessing (HyperMesh v. 11.0)

In the preprocessing part, the undamaged composite sandwich beam is constructed and defined in terms of an ABAQUS input file. To define the orthotropic properties of the composite face sheet and the core properties, these material properties for both the face sheet (E-glass/epoxy) and the core (End-grain balsawood) were determined from preliminary tests (Tables 4.1 and 4.2) and then inserted into the material component of the finite element model. The model of the undamaged balsawood core/glass fiber beam was created for FEA. Due to the

symmetry of composite sandwich beam geometry, boundary conditions, and loading, only 1/2 of the gage length (25.4 mm) of CLC test model was considered in order to reduce the computational time. Eight-node three dimensional elements (C3D8I) were used to model both the E-glass/epoxy face sheet and end-grain balsawood. Element length of 0.45 mm is maintained in the sandwich beam model. The face sheet was designed as one layer and represented by one brick element through the thickness and the core was designed as seven layers and modeled by seven brick elements along half of the thickness. The development of finite element model involved meshing of the all surfaces of the geometric model and resulted in the creation of 6720 elements with 8208 nodes. Finite element model mesh of the entire and half of the undamaged sandwich beam was shown in Fig. 5.5.
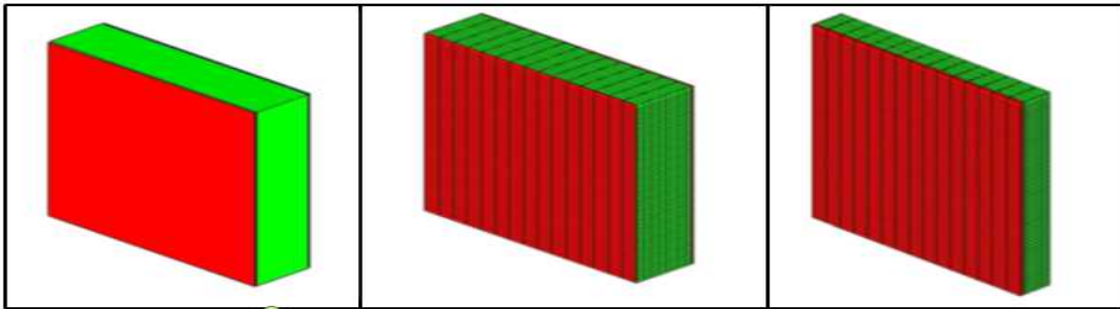
Fig. 5.5. Finite element mesh of the entire and half of the composite sandwich beam

The undamaged composite sandwich beam was subjected to the uniform load located at the top surface of the beam. The load was applied in the vertical direction (y-direction) under a displacement boundary condition and the boundary

condition considered in this simulation was that all nodes at the bottom surface of the beam were constrained in three directions x, y, and z as shown in Fig. 5.6. As the main interest of the finite element work to obtain the maximum interfacial stress and the normal stress distribution along the thickness of the undamaged sandwich beam, the displacement boundary condition with the maximum displacement (1.26 mm) reached in our experiment was the end of the elastic limit of the beam.
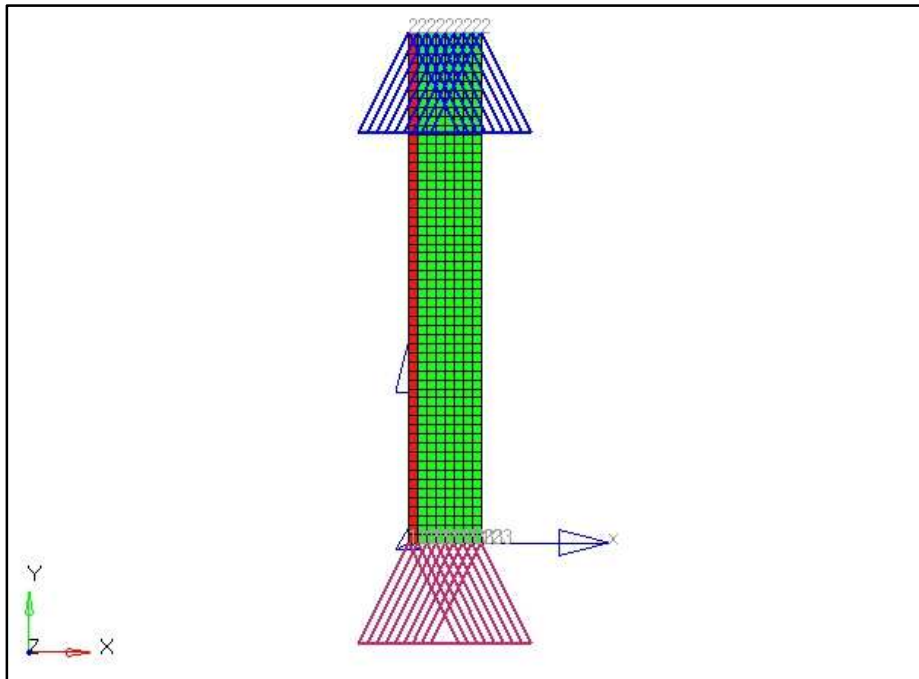
Fig. 5.6. Finite element analysis model

5.2.2 Simulation (ABAQUS/Standard 6.11)

In ABAQUS, there are two different codes including ABAQUS/Standard and ABAQUS/Explicit. In this case ABAQUS/Standard was used for the simulation of

the undamaged composite sandwich beam. In this simulation stage, the numerical problem defined in the model was solved by ABAQUS/Standard and ABAQUS generates a number of different files including the output result file which was used in the post-processor stage. The simulation may take time from seconds to days to complete an analysis run, therefore, it depends upon the complexity of the problem being analyzed and the power of the computer utilized for the analysis.

5.2.3 Post-Proceeding (HyperView/HyperMesh v 11.0)

HyperView and/or HyperMesh v 11.0 both can be used as a post-processor. In the present study, HyperMesh v 11.0 was used to visualize the results graphically. One file generated by the simulation was the (.fil) file, and it was converted into (.res) file which was a HyperMesh result file. Then, the result file was imported into the HyperMesh v 11.0 environment. In the post-processor stage, various output results such as displacements, strains, stresses etc. can be evaluated based on the input file controlling commands. HyperMesh v 11.0 has a variety of options for displaying the results of FEA, including color contour plots, deformed shape plots, animations etc. The vertical stress distribution along the thickness of the undamaged sandwich beam was plotted at the maximum displacement and the maximum facing/core interface stress value determined to understand the behavior of the sandwich beam under in-plane compressive load in order to meet design requirements in applications.

CHAPTER SIX

RESULTS AND DISCUSSION

6.1 Impact Tests

Initial impact tests with energies between 5 J and 17J were performed to produce visible impact damage for subsequent fatigue loading. The existence of the threshold energy to cause impact damage was found to be approximately 8 J for this class of composite sandwich beams. All specimens were impacted with energies 8.8 J and the impact-induced damage was principally manifested in the form of delaminations. The damage area induced by the impact load was captured by a digital camera and measured by image J software. The average delamination area of impacted sandwich beams was 381.52 mm^2 with a standard deviation (STD) of 10.32 mm^2 for total of twelve samples. Typical impact damage can be visually clearly observed from the digital images (Fig. 6.1). The end-grain balsa wood core facilitates development of this delamination well.

6.2 Compression Static Tests

Impacted and non-impacted specimens were tested under static compression to measure the strength of sandwich beams and the limits required for fatigue. Typical load-displacement responses for impacted and non-impacted sandwich beams are shown in Fig. 6.2. These data were plotted according to the data recorded in the MTS machine. Therefore, load displacement data, for damaged and undamaged specimens, were converted into compressive stress as
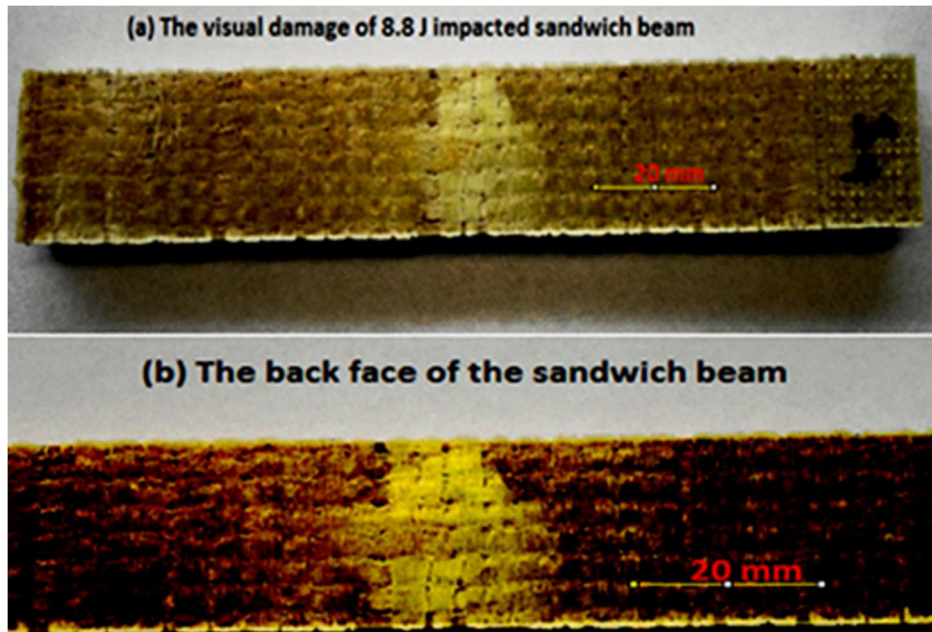
Fig. 6.1. Examples of the visual damage caused by impacts
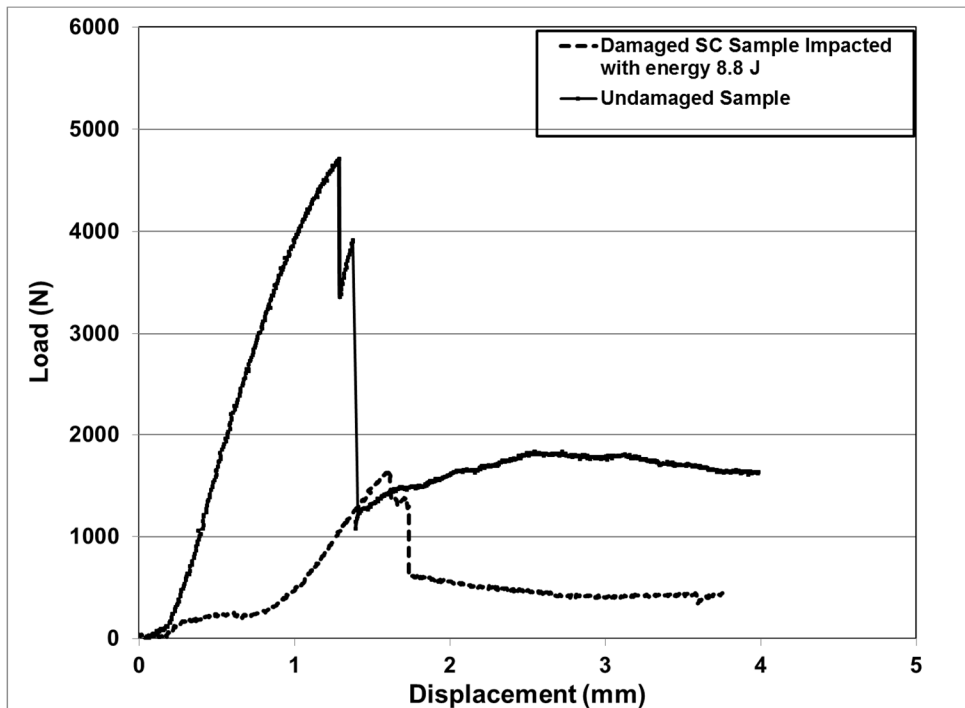
Fig. 6.2. Typical in-plane Static compression load-Displacement responses for undamaged and damaged specimens

function of in-plane strain of these beams. Typical stress-strain responses for damaged and undamaged specimens are shown in Fig. 6.3. The stress was calculated by dividing the compressive load by the in-plane cross section area of sandwich composite specimen, whereas the strain was calculated by dividing displacement by the 25mm gauge length at the middle of the sample. The stress-strain response is almost linear until the maximum stress is reached in both damaged and undamaged specimens. Then, stress suddenly drops, and strain remains constant. After that, stress slightly increases or remains constant with increase in strain and finally material fails. The average ultimate compressive strength (σ_{ul}) was on average 26.1 MPa with a standard deviation (STD) of 0.52 MPa for unimpacted specimens and 8.15 MPa with a standard deviation (STD) of 0.69 MPa for impacted ones. From the comparison of stress-strain curves, much effect of the impact damage is observed on maximum compressive strength. The residual strength of impacted specimens was only 31% of maximum compressive strength of non-impacted specimens. The damage state and average of the failure load for composite sandwich beams is summarized in Table 6.1. In Fig. 6.3, peak stresses occur at 0.054 and 0.069 strain values for the undamaged and damaged sandwich beams, respectively. For the undamaged specimen, face sheet damage with some delamination is followed by bulk core shear band formation leading to failure of the specimen (Fig. 6.4). The impact damaged sample exhibits a more complex damage as shown in Fig. 6.5. In this case, there is local core shear on a

smaller scale which is linked from two edges via the impact damage at its perimeter resulting in finally complete failure of the sample. However, significant out of plane deformation of the rear face sheet (major delamination) are observed during the entire loading process and it appears that the face sheets are severely damaged due to fiber breaks carrying some load until failure. Fig. 6.5 depicts the face sheet/core delamination growth, which was the major event during in-plane compressive loading. The sequence of the entire growth of delamination was visually observed using a digital camera up to final failure.
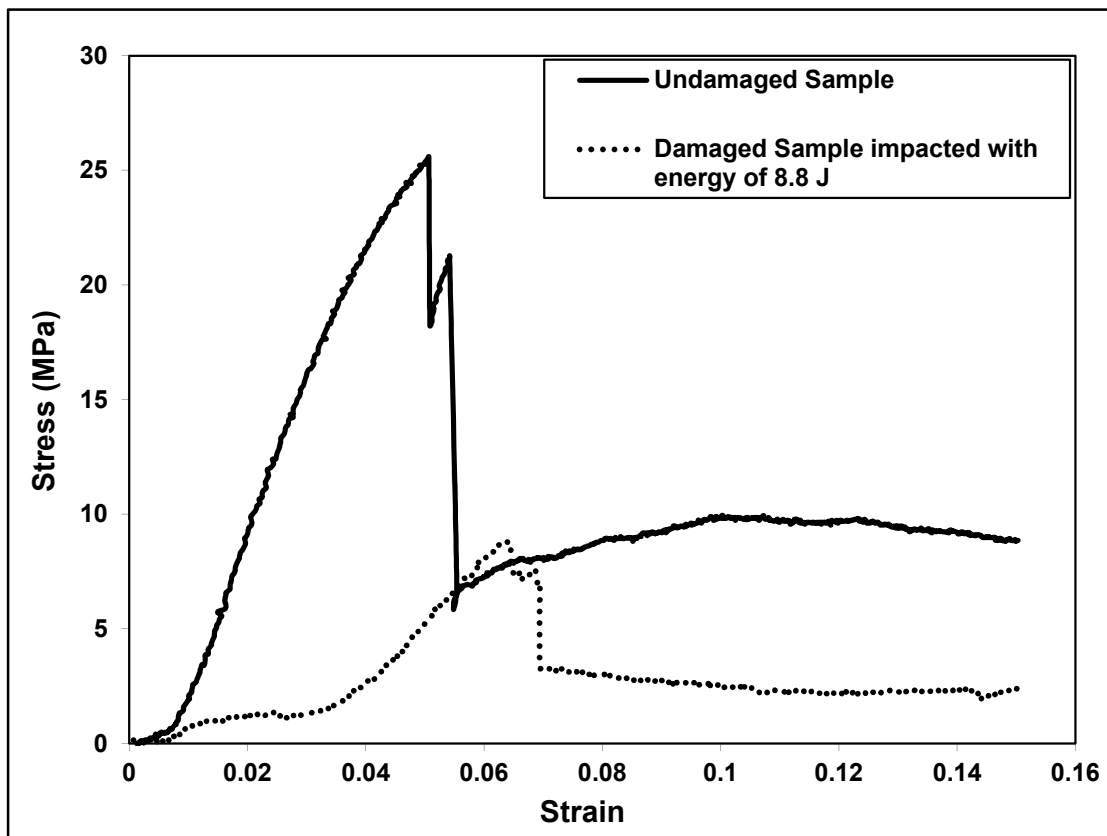
Fig. 6.3.   Typical in-plane static compression stress-strain responses of undamaged and damaged specimens

Table 6.1. Damage state and average failure load for this class of sandwich composites

Damaged state (J)	Average failure load (MPa)	Residual load carrying capacity
8.8	8.15	31%
Undamaged	26.1	-
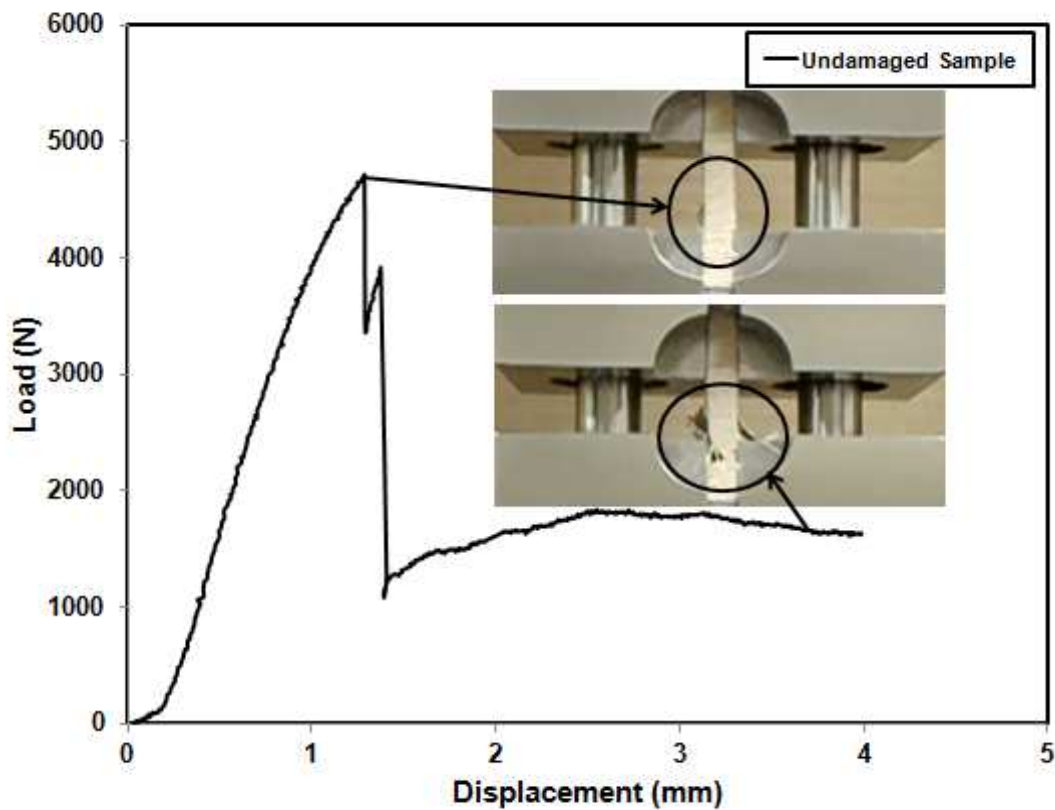
Fig. 6.4. Typical in-plane static compression load-displacement response of showing failure modes of undamaged sandwich beams
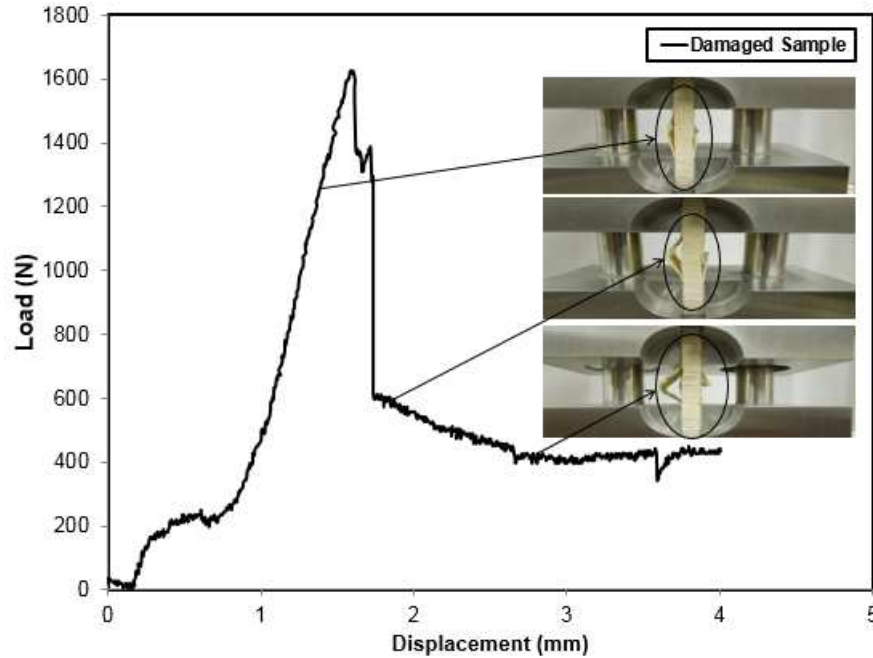
Fig. 6.5. Typical in-plane static compression load-displacement response
showing face sheet delamination during various stages of compression

6.2.1 Experimental and Analytical Results of P_{cr}

For experimental work, videos were recorded for each compression test of

the delaminated composite sandwich beam from the beginning to the end of the

test. As it was observed in experiments and these videos, each specimen was

compressed between two platens, and the face sheet delamination starts to buckle

at a certain time when the axial compressive load reaches to P_{cr}. This was a clear

indication of the initiation of the buckling of the specimen. Since the time was

known for this event and obtained from the video recording, load can be traced

back from this time scale in experimental data. To get reliable data, six

delaminated specimens were tested to obtain P_{cr}. Typical critical buckling load measured experimentally is shown in Fig. 6.6 (certain time is around 43 Sec.).
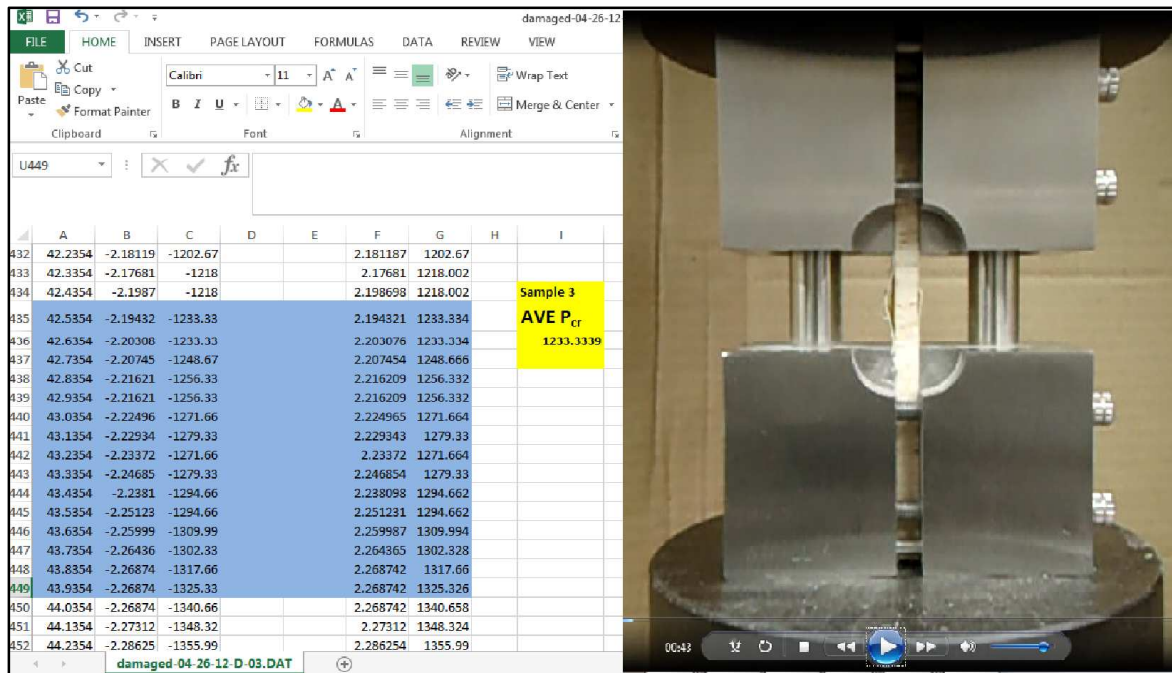
Fig. 6.6. Typical critical buckling load measured experimentally
(P_{cr}, average = 1233.33 N)

For analytical approach, critical buckling loads were calculated based on equations (3.49), (3.50), and (3.51) and material properties given in Tables 4.1 and 4.2. Beam dimensions used for this calculation were: *2l* = 152.4 mm, *b* = 25.4 mm, *c* = 6.35, *f₁* = *f₂* = 0.45 mm. The length of the delamination (*2a*) before and after the compression test was measured by software image J software as shown in figure 6.7. Critical buckling loads of delaminated composite sandwich beams determined by analytical and experimental techniques are listed in Table 6.2. The correlation between experimental and analytical results is very good.
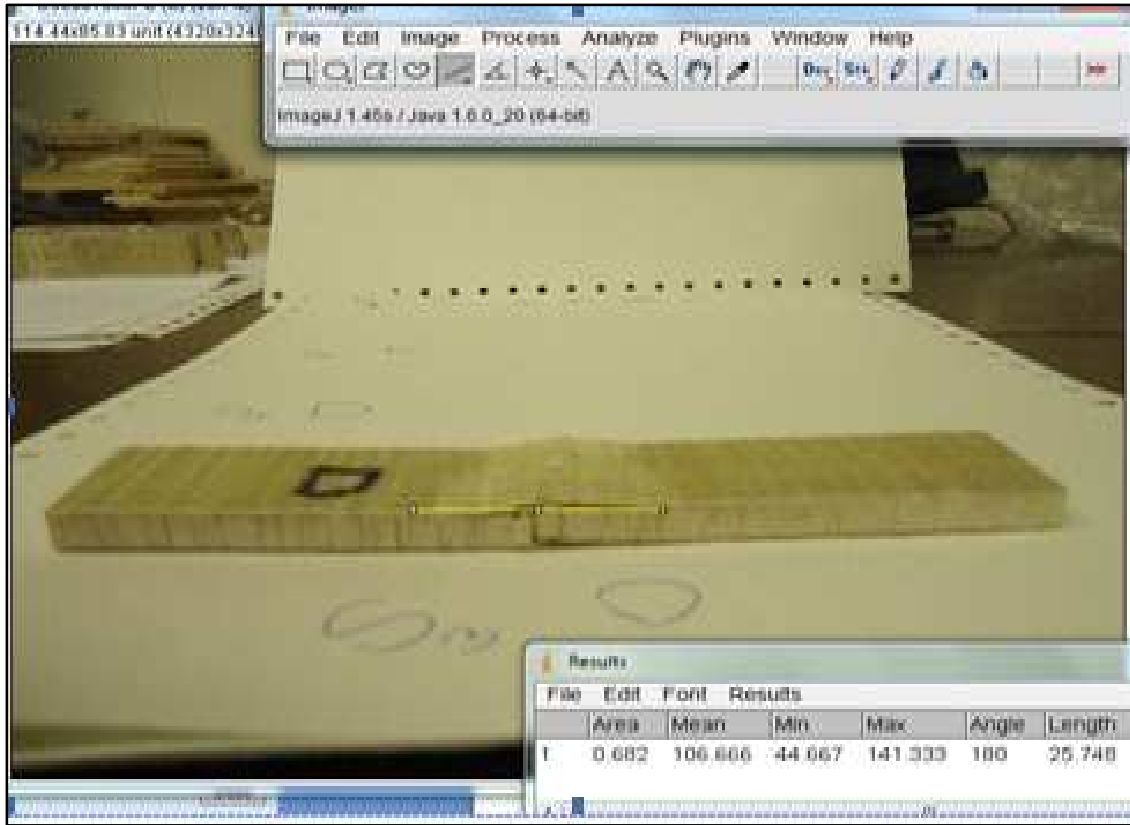
Fig. 6.7. Delamination length measured by Image J software after compression test

Table 6.2. Comparison of critical buckling loads determined from two different techniques for damaged beams

Sample ID	Analytical P_{cr} (N)	Experimental P_{cr} (N)
D1	1055.91	1233.33
D2	1079.31	1201.67
D3	1104.49	1320.86
D4	1105.29	1289.28
D5	1131.26	1378.54
D6	1064.48	1168.46

6.3 Compression-Compression Fatigue Tests

Facing and core stresses were determined by using the elementary mechanics of materials for predicting the independent modulus of balanced orthotropic face sheets and the core material which form the composite sandwich structure in the case of the longitudinal normal compressive stress . The response for the composite sandwich beam using in this work is governed by the effective longitudinal modulus (E_1). Static equilibrium requires that the total resultant force on the sandwich structure must equal the sum of the forces acting on the face sheet and the core and this can be expressed to give a "rule of mixture" for longitudinal stress in the following equation:

$$\sigma_{s1} V_1 = \sigma_{f1} V_f + \sigma_{c1} V_c \tag{6.1}$$

Where subscripts s, f, and c refer to sandwich composites, face sheet, and the core, respectively, and the second subscript refers to the direction. Since the area fractions are equal to the corresponding volume fractions, equation (6.1) can be rearranged and then become:

$$\sigma_{s1} A_1 = \sigma_{f1} A_f + \sigma_{c1} A_c \tag{6.2}$$

$$\bar{\sigma}_{s1} = \bar{\sigma}_{f1} v_f + \bar{\sigma}_{c1} v_c \tag{6.3}$$

Under the assumption that the balsa wood may be categorized as transversely isotropic for most practical purposes and that the materials follow Hook's law:

$$\bar{\sigma}_{s1} = E_1 \bar{\epsilon}_{s1} \; ; \quad \bar{\sigma}_{f1} = E_{f1} \bar{\epsilon}_{f1} \; ; \quad \bar{\sigma}_{c1} = E_{c1} \bar{\epsilon}_{c1} \tag{6.4}$$

By substituting the stresses from equation (6.4) into equation (6.3) which becomes:

$$E_1 \bar{\epsilon}_{s1} = E_{f1} \bar{\epsilon}_{f1} \upsilon_f + E_{c1} \bar{\epsilon}_{c1} \upsilon_c \qquad (6.5)$$

The key assumption is that the average strains in the sandwich composite, face sheet and the core along the 2 direction (the compressive load direction) are equal:

$$\bar{\epsilon}_{s1} = \bar{\epsilon}_{f1} = \bar{\epsilon}_{c1} \qquad (6.6)$$

Substitution of equation (6.6) in equation (6.5) and then the longitudinal stress can be obtained:

$$E_1 = E_{f1}\upsilon_f + E_{c1}\upsilon_c \qquad (6.7)$$

By using equations (6.3), (6.4), and (6.7) the facing and the core stresses for undamaged and damaged samples were calculated and then summarized in Tables 6.3 and 6.4.

The experimental results of compression-compression fatigue tests performed on balsawood core/glass fiber beams at different load levels, r, are listed in terms of number of cycles to failure in Table 6.5 for non-impacted specimens, and Table 6.6 for impacted specimens. Fatigue test data of impacted and unimpacted sandwich beams were processed in the forms of relationships either maximum compressive stress (σ_{min}) or facing stress versus number of cycles (N) in Fig. 6.8 and Fig. 6.9, respectively. It is revealed from these figures that the compression fatigue performance decreases with the increase of maximum imposed stresses as expected.

In order to clarify the amount of fatigue strength degradation the S-N were plotted using an ordinate normalized by ultimate compressive strengths of the

specimens (σ_{min}/σ_{ul}) as shown in Fig. 6.10. This figure shows the number of cycles to failure increases as the load level decreases for both damaged and undamaged specimens. What is more interesting is that the rate of degradation is similar in terms of the negative slope lines (if drawn) of the fatigue data in this figure. Once delamination is induced in the samples, either via impact or via compressive load, the degradation is controlled by delamination growth and has similar rates. It is the relative high load that is important for delamination growth and our focus was to investigate the fatigue response within 40% of max load (CAI). Since polymer composite fatigue mechanisms are controlled by damage growth and corresponding load distribution and not "plasticity" as in metals, if initial damage can be avoided, long fatigue life can be expected. Therefore, our primary focus is "delamination growth" at relative higher stresses in relation to the strength of the composite. Delamination growth is not seen for these this class of sandwich composites at stress levels at 0.4 load level. Implication is that even with impact damage, a structure may survive with no further degradation if local design stresses can be kept below this "level".

Tables 6.3. Facing and core compressive stresses for undamaged specimens

σ_1/σ_{max}	σ_1, MPa	ε_1	E_1,MPa	E_{c1},MPa	σ_{C1},MPa	E_{f1},MPa	σ_{f1}, MPa
0.1	2.61	0.002779	939.20	23.50	0.065	7400	20.56
0.2	5.22	0.005558	939.20	23.50	0.131	7400	41.13
0.3	7.83	0.008337	939.20	23.50	0.196	7400	61.69

σ_1/σ_{max}	σ_1, MPa	ε_1	E_1,MPa	E_{c1},MPa	σ_{C1},MPa	E_{f1},MPa	σ_{f1}, MPa
0.4	10.44	0.011116	939.20	23.50	0.261	7400	82.26
0.5	13.05	0.013895	939.20	23.50	0.327	7400	102.82
0.6	15.66	0.016674	939.20	23.50	0.392	7400	123.39
0.7	18.27	0.019453	939.20	23.50	0.457	7400	143.95
0.8	20.88	0.022232	939.20	23.50	0.522	7400	164.51
0.9	23.49	0.025011	939.20	23.50	0.588	7400	185.08
1	26.10	0.027790	939.20	23.50	0.653	7400	205.64

Table 6.4. Facing and core compressive stresses for damaged specimens

σ_1/σ_{max}	σ_1, MPa	ε_1	E_1,MPa	E_{c1},MPa	σ_{C1},MPa	E_{f1},MPa	σ_{f1}, MPa
0.1	0.82	0.000869	939.20	23.50	0.020	7400	6.43
0.2	1.63	0.001738	939.20	23.50	0.041	7400	12.86
0.3	2.45	0.002606	939.20	23.50	0.061	7400	19.29
0.4	3.26	0.003475	939.20	23.50	0.082	7400	25.71
0.5	4.41	0.004693	939.20	23.50	0.110	7400	34.73
0.6	4.90	0.005213	939.20	23.50	0.123	7400	38.58
0.7	5.71	0.006082	939.20	23.50	0.143	7400	45.01
0.8	6.53	0.006951	939.20	23.50	0.163	7400	51.43
0.9	7.34	0.007818	939.20	23.50	0.184	7400	57.86
1	8.16	0.008688	939.20	23.50	0.204	7400	64.29

Table 6.5. Compression-Compression fatigue results for non-impacted specimens

Specimen ID	$\sigma_{min}/\sigma_{ult}$	Maximum compressive stress, MPa	Facing Stress, σ_f, MPa	Number of cycles to failure
F-UD-1	1	26.10	205.64	0
F-UD-2	1	24.55	193.56	0
F-UD-3	1	24.02	189.24	0
F-UD-4	0.7	18.27	143.95	155006
F-UD-5	0.7	18.27	143.95	160000
F-UD-6	0.7	18.27	143.95	149027
F-UD-7	0.6	15.66	123.39	301254
F-UD-8	0.6	15.66	123.39	314258
F-UD-9	0.6	15.66	123.39	330125
F-UD-10	0.5	13.05	102.82	945002
F-UD-11	0.5	13.05	102.82	961258
F-UD-12	0.5	13.05	102.82	No failure
F-UD-13	0.4	10.44	82.26	No failure
F-UD-14	0.4	10.44	82.26	No failure
F-UD-15	0.4	10.44	82.26	No failure

Table 6.6. Compression-Compression fatigue results for impacted specimens

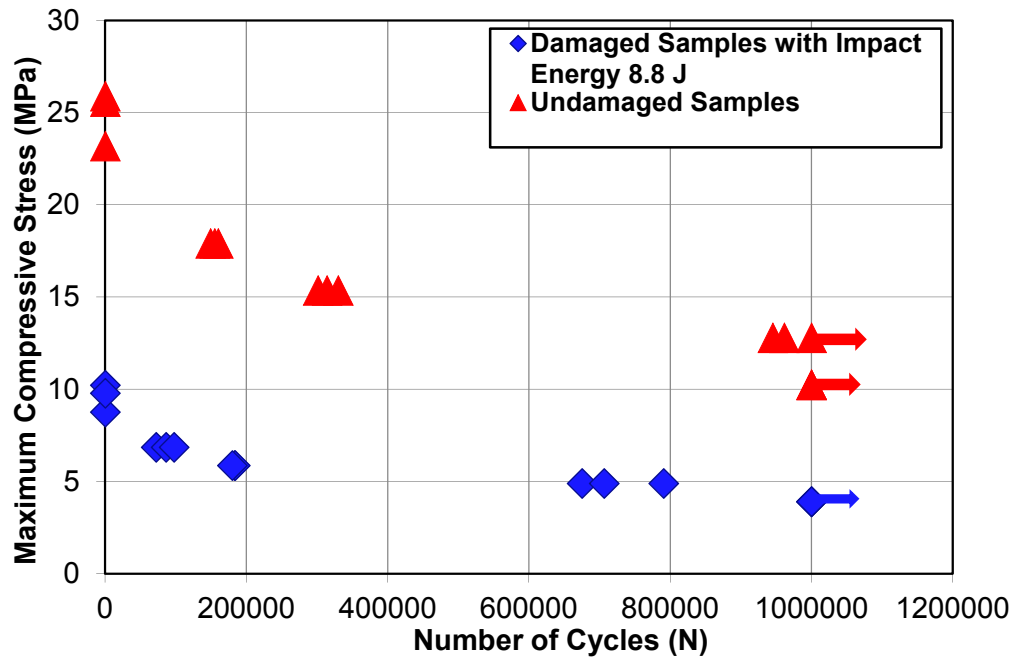| Specimen ID	$\sigma_{min}/\sigma_{ult}$	Maximum compressive stress, MPa	Facing Stress, σ_f, MPa	Number of cycles to failure
F-D-1	1	8.16	64.29	0
F-D-2	1	8.11	63.89	0
F-D-3	1	7.67	60.43	0
F-D-4	0.7	5.71	45.01	72235
F-D-5	0.7	5.71	45.01	86145
F-D-6	0.7	5.71	45.01	97320
F-D-7	0.6	4.9	38.58	182968
F-D-8	0.6	4.9	38.58	184000
F-D-9	0.6	4.9	38.58	179800
F-D-10	0.5	4.41	34.73	675120
F-D-11	0.5	4.41	34.73	790541
F-D-12	0.5	4.41	34.73	706515
F-D-13	0.4	3.26	25.71	No failure
F-D-14	0.4	3.26	25.71	No failure
F-D-15	0.4	3.26	25.71	No failure

Fig. 6.8. Maximum compressive stress (S_{min}) versus number of cycles (N) for impacted and non-impacted samples (R=10)
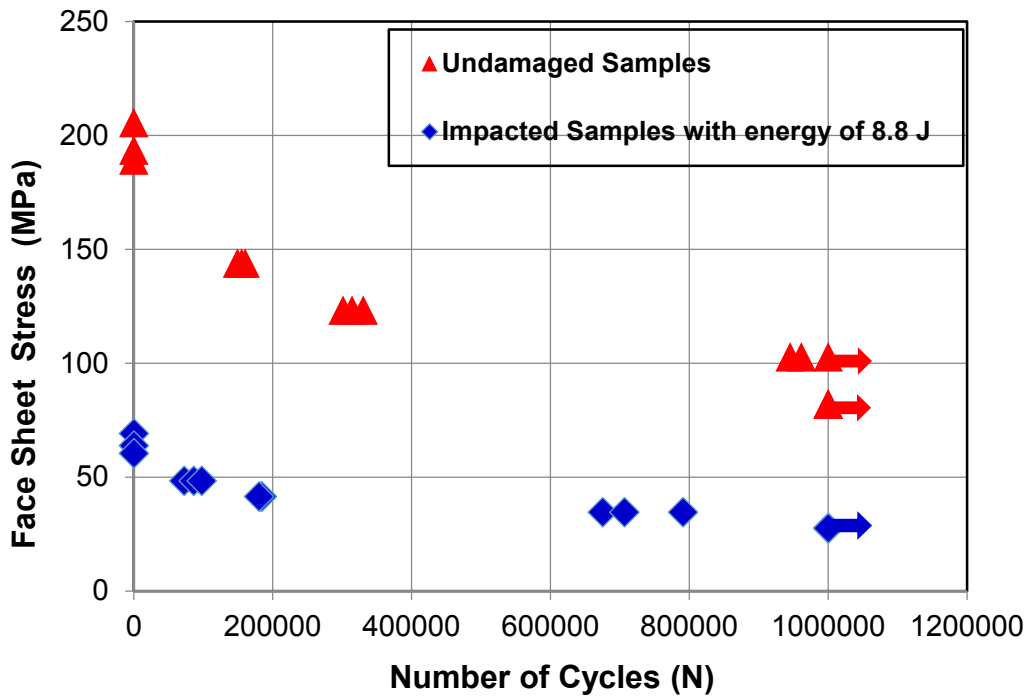

Fig. 6.9. Face sheet stress versus number of cycles (N) for impacted and non-impacted samples (R=10)
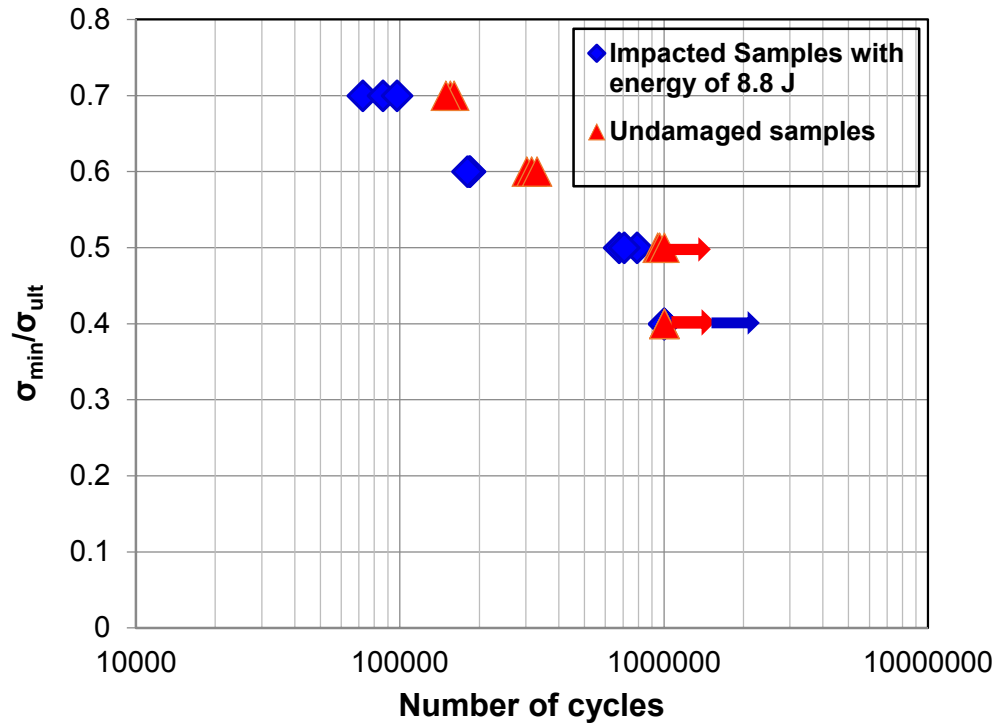
Fig. 6.10. Normalized stress ($\sigma_{min}/\sigma_{ult}$) versus number of cycles (N) for R=10

One of the most commonly method used to study the progression of impact damage during the cyclic fatigue is noticing and recording changes in stiffness of sandwich composites. The dynamic stiffness of the specimens with impact damage was determined from the hysteresis loops at specific number of cycles during the fatigue life at 0.4, 0.5 and 0.6 load levels and three samples were tested for each case. The typical stiffness versus number of cycles at different load levels was plotted on different graphs respectively as shown in Fig. 6.11, Fig. 6.12, and Fig. 13. It was observed that the stiffness curve was almost flat throughout the fatigue life at 0.4 load level (see Fig. 6.11). At 0.5 and 0.6 load levels, the stiffness curves sloped downwards with increasing numbers of cycles. The stiffness curve

at 0.6 load levels exhibited a more steeply declining that ones at 0.5 load levels as shown in Fig. 6.12 and Fig. 6.13. The rate of stiffness degradation depends on load levels during fatigue tests. The stiffness reduction showed a marked difference at higher load level compared to small values of load levels (Fig. 6.14).

A Gaertner microscope was utilized to monitor the delamination growth, and a digital camera was used to capture modes of failure throughout the fatigue test. Delamination length as a function of number of cycles is shown in Fig. 6.15 for three load levels, 50%, 60%, and 70% of CAI. As shown in this figure, the delamination growth curve was almost flat up to ~1000 cycles at 70% CAI, and then the rapid growth of delamination begins leading to final failure. In Fig. 6.15, a delay in delamination growth is seen up to about 10000 cycles for both 60% and 50% CAI, and then delamination growth increases with increasing number of cycles with less rapid growth exhibited for the 50% case. Fig. 6.16 shows the observed fatigue failure modes sequence of an impacted sandwich specimen (0.6 load level). This impacted specimen with energy of 8.8 J resulting in delamination cyclically loaded to a maximum compressive stress of 5.18 MPa. The fatigue life of this specimen was 182982 load cycles. Fig. 6.16 explains the impact damage growth of the back surface of the specimen during the fatigue test. Fatigue failure was induced predominantly by the propagation of delamination in the loading direction. Failure initiated with delamination and then followed by core shear and skin failure (Fig. 6.16).
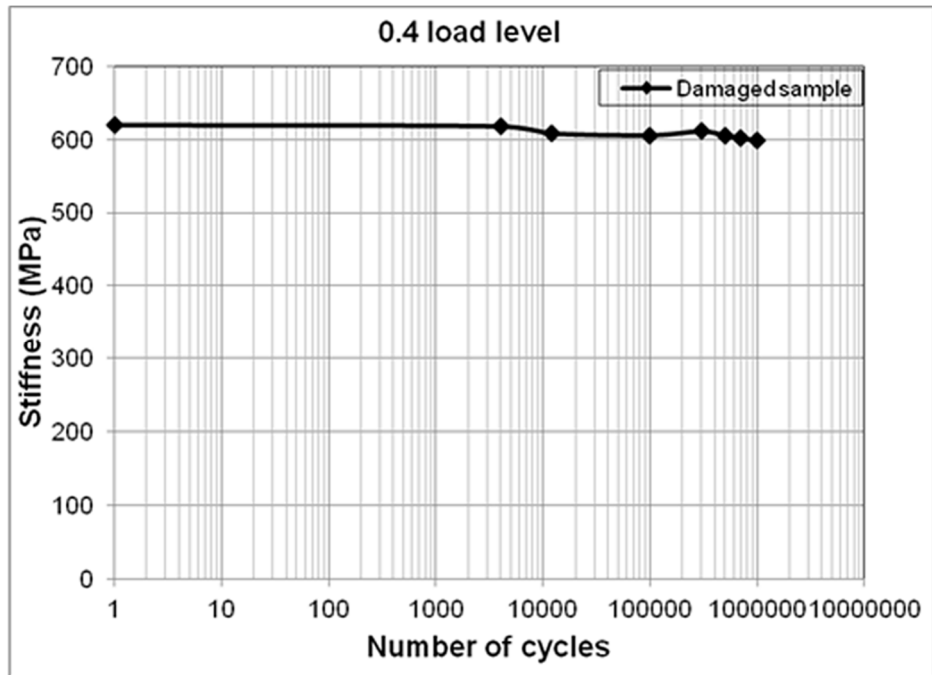
Fig. 6.11. Typical graphs showing changes in stiffness of sandwich beams during fatigue tests at the load level 0.4
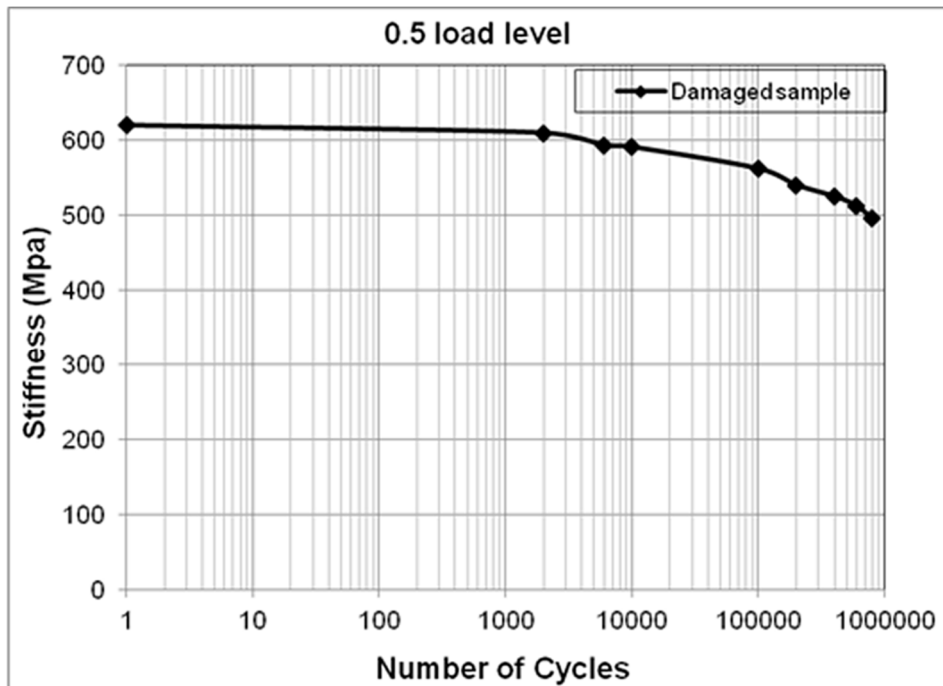
Fig. 6.12. Typical graphs showing changes in stiffness of sandwich beams during fatigue tests at the load level 0.5

Fig. 6.13. Typical graphs showing changes in stiffness of sandwich beams during fatigue tests at the load level 0.6

Fig. 6.14. Typical graphs showing changes in stiffness of sandwich beams during fatigue tests at 40%, 50%, and 60% of ultimate stress
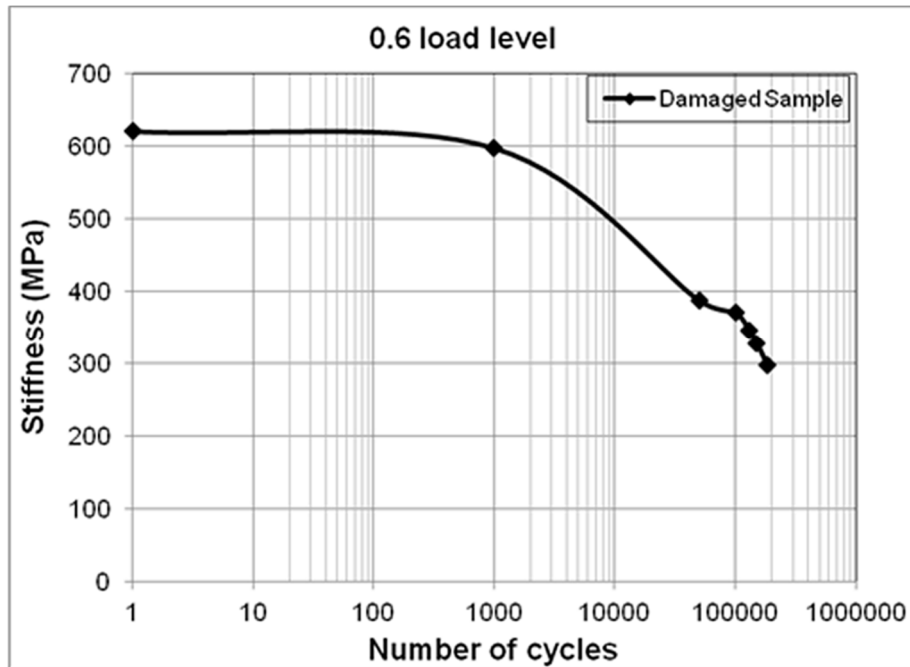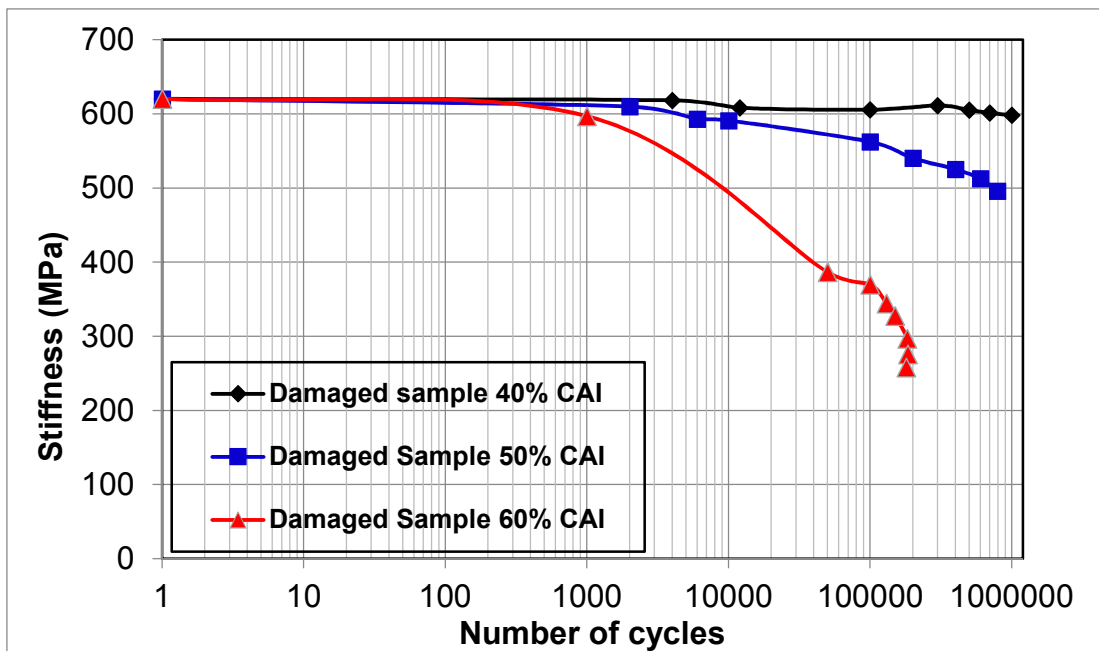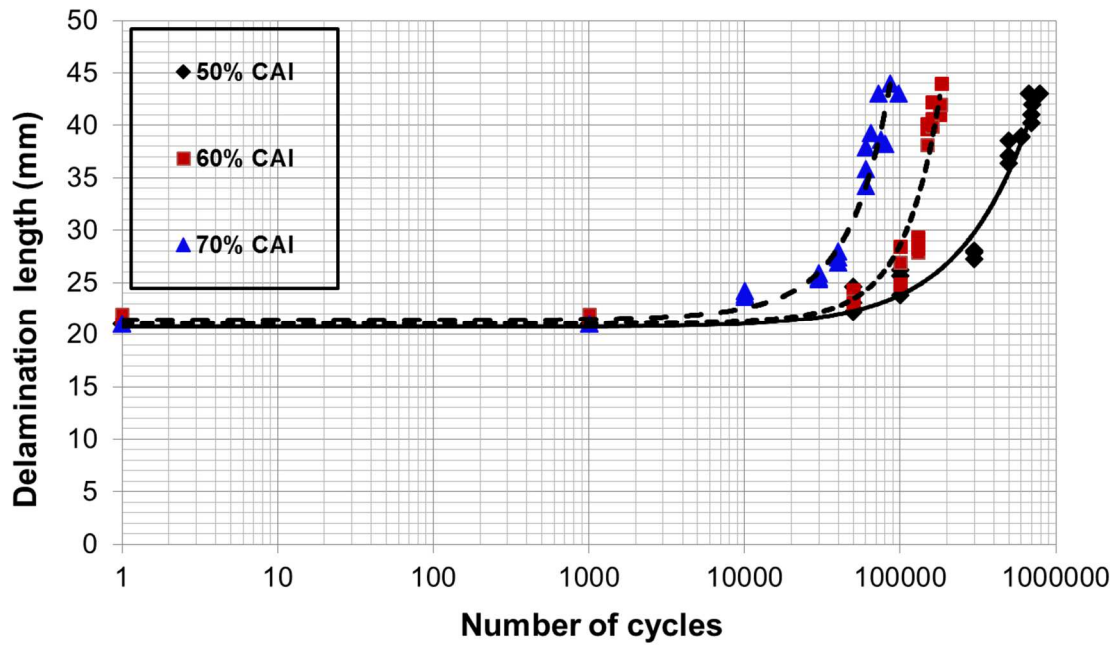
Fig 6.15. Delamination growth in compression-compression fatigue for Sandwich beams at 50%, 60% and 70% CAI as a function of number of cycles
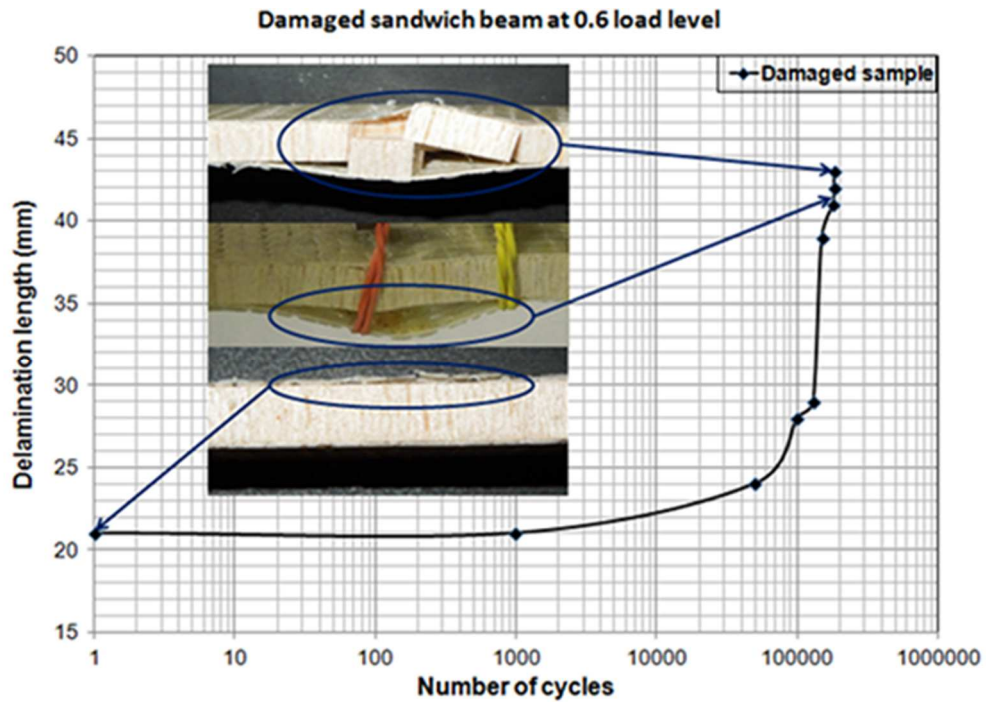

Fig. 6.16. Failure modes sequence in sandwich beams under compression fatigue loading

6.4 Finite Element Analysis Results

As facing and core stresses were calculated by using the analytical approach, FEA was performed to predict the stress distribution including the interfacial stress along the thickness of the sandwich beam subjected to in-plane compressive load. In this analysis on this model, the compressive stress distribution along the thickness of the undamaged sandwich beam was investigated at the maximum compressive load which is represented in this model by maximum displacement (1.26mm) reached in the experimental work.

The stress distribution along the thickness is shown in Fig. 6.17. The facing and core stresses presented first and then compared with the analytical result listed in Table 6.3. The result shows very good agreement between the analytical calculation and ABAQUS finite element analysis. The maximum facing stress calculated analytically was 205.64 MPa while the value of the facing stress obtained from FEA for the undamaged composite sandwich beam was 199.08 MPa. As can be seen from the Fig. 6.17, the facing/core interface stress value of the point (x = 0.45 mm, y = 12.7 mm) was determined and it was 99.08 MPa at the thickness of 0.45 mm. Fig. 6.17 shows the in-plane normal stress distribution along the thickness of the point (x = 0, y = 12.7 mm). The maximum interfacial stress value was determined by FEA as shown in this figure at the thickness of 0.45 mm. As can be seen from the Fig 6.17, the in-plane stress curve discontinues at the face sheet core interfaces for stress distribution which was determined

analytically. Also it can be observed that in-plane stresses in the core are very small in comparison with those obtained in the face sheet.
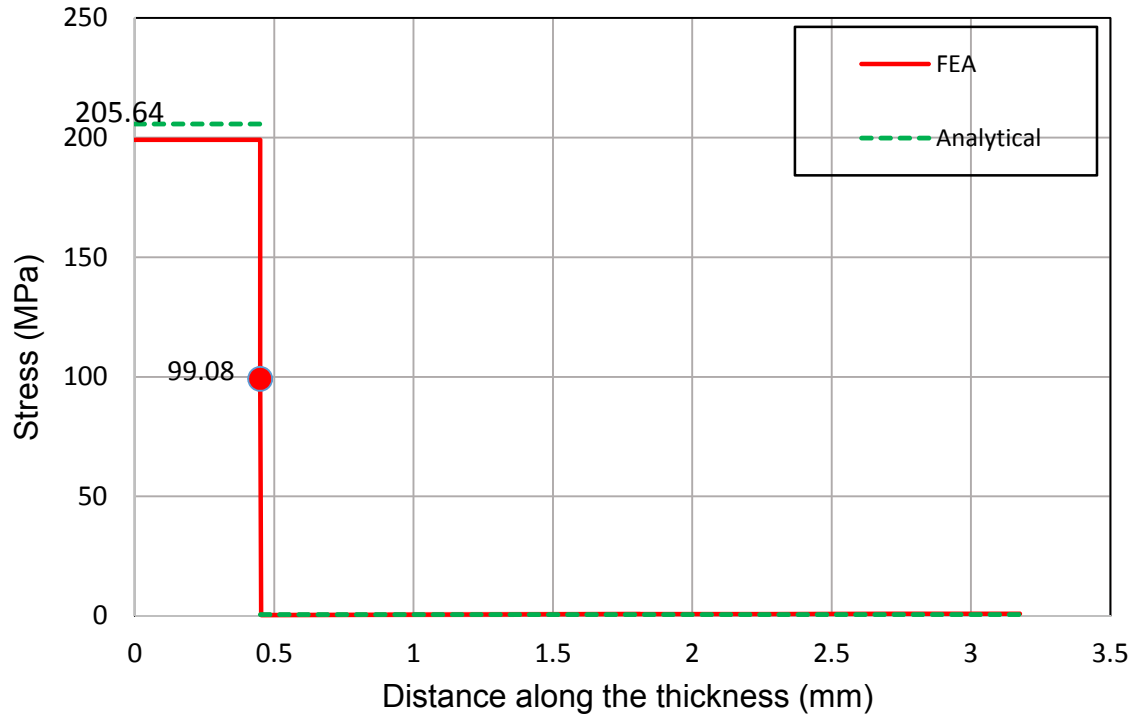
Fig. 6.17. Stress distribution obtained along the thickness of the undamaged composite sandwich beam

CHAPTER 7

CONCLUSIONS AND RECOMMENDATIONS

7.1 CONCLUSIONS

In this research work, the effect of impact damage on in-plane buckling and compression-compression fatigue behavior were investigated for a new composite sandwich structure manufactured with glass fiber laminates as face sheets and with end-grain balsa wood as core. These composite sandwich panels can be used in many applications such as automotive industries. The conclusions made from this investigation:

- **Impact response**

    a. Initial impact tests with energies between 5J and 17J were conducted first and then Impact tests at energy level of 8.8 J – slightly above the threshold level for damage were carried out In preparation for the compression static and compression-compression fatigue tests.

    b. Inspection of the skin damage and delamination at core/skin interface can be observed through visual inspection for the end-grain balsawood core which facilitates development of this delamination well.

- **Compression static tests and critical buckling load (P_{cr})**

    a. Compression static tests for damaged and undamaged composite sandwich specimens were carried out and compressive strength and residual strength were obtained.

b. It was found that the strength of sandwich composite beams reduced about 69% after impact at 8.8 J.

c. An analytical and experimental approaches were used to investigate buckling of delaminated composite sandwich beams and predict the critical buckling load of these beams.

d. The correlation between Analytical (Hwu &Hsieh) and experimental results are very good in the case critical buckling load (P_{cr}) of delaminated composite sandwich beams.

- **Fatigue response**

  a. Compression-Compression fatigue tests were performed for impacted and non-impacted composite sandwich beams.

  b. Fatigue test data of impacted and unimpacted sandwich beams were processed first in the forms of relationships either maximum compressive stress (S_{min}) or facing stress versus number of cycles (N), and then the S-N were plotted to clarify the amount of fatigue strength degradation.

  c. The number of cycles to failure increases as the load level decreases for both damaged and undamaged specimens.

  d. Compression fatigue performance for non-impacted sandwich beams is significantly better than impacted ones.

e. Once delamination is induced in the samples, either via impact or via compressive load, the degradation is controlled by delamination growth and has similar rates.

f. Delamination growth is not seen for this class of sandwich composites at in-plane stress levels at 40% of ultimate stress, and a structure may survive with no further degradation if local design stresses can be kept below this "level".

g. The stiffness reduction showed a marked difference at higher load level compared to small values of load levels and it was observed that any appreciable stiffness loss in fatigue does not occur at CAI values of less than 50%.

h. Fatigue strength degradation rate was similar between the impacted and non-impacted sets of samples and was likely due to delamination controlled damage progression in both cases.

i. There was significant degradation of fatigue life due to impact damage in relation to undamaged composites.

j. In sandwich composite with soft core such as end-grain balsa, failure initiates with delamination which can be followed by either skin or core failure during fatigue.

- **Finite Element Analysis**

  a. The analytical and finite element results show very good agreement for facing and core stress values.

b. The facing/core interface stress value for undamaged composite sandwich beam was determined by using ABAQUS FEA.

c. It can be observed that in-plane normal stresses in the core are very small in comparison with those obtained in the face sheet.

7.2 RECOMMENDATIONS

The continued research could be further developed in number of ways:

- The effect of impact damage area on compression-compression fatigue performance of end-grain balsawood core/glass fiber composite sandwich composites can be studied.

- The effect of impact damage on compression-compression fatigue performance of sandwich composites made from 0/90 E-glass/epoxy face sheets over regular balsa wood core can be investigated.

- The effects of the face sheet and the core thicknesses on compression-compression fatigue performance should be studied.

- Non-destructive evaluation techniques should be used to detect the damage induced by impact.

- In future work, Finite element Analysis is needed to investigate and predict the stress distribution and the interfacial stress in the case of damaged composite sandwich beams.

- Finite element analysis can be used to investigate linear buckling analysis and non-linear post buckling analysis and predict critical buckling loads (P_{cr}).

REFERENCES

[1] Jones, R. M., 1999. *Mechanics of composite materials*, Published by Taylor and Francis, Second Edition, ©1975.

[2] Zenkert, D., 1995. *An introduction to sandwich construction,* Solihull (UK), Engineering Materials Advisory Services Ltd. (EMAS), [ISBN: 0947817778].

[3] Achilles P., (1998). *Design of sandwich structures,* Ph.D. Thesis, Cambridge University, UK.

[4] Gibson, RF., 2007. *Principles of composite material mechanics*, Second edition. CRC Press, [ISBN 0824753895].

[5] Yin, W.L., 1958. "The effects of laminated structure on delamination buckling and growth," Journal of Composite Materials 22, (6), pp. 502-517.

[6] Chai, H., Babcock, C.D., and Knauss, W.B., 1981. "One-dimensional modeling of failure in laminated plates by delamination buckling," International Journal of Solids and Structures 17, 1069–83.

[7] Simitses, G.J., Sallam, S., and Yin, W.L., 1985. "Effect of delamination of axially loaded homogeneous laminated plates," AIAA Journal, 1437–44.

[8] Chai, H., and Babcock, C.D., 1985. "Two dimensional modeling of compressive failure in delaminated laminates," Journal of Composite Materials 19, pp. 67–98.

[9] Yin, W.L., Sallam, S.N., and Simitses, G.J., 1986. "Ultimate axial load capacity of a delaminated beam-plate," AIAA Journal 24(1), 123–8.

[10] Minguet, P., Dugundji, J., and Lagace, P.A., 1987. "Buckling and Failure of Sandwich Plates with Graphite-Epoxy Faces, and Various Cores," Journal of Aircraft, 25(4), pp. 372-379.

[11] Kardomateas, G.A., 1990. "Post-buckling Characteristics in Delaminated Kevlar/Epoxy Laminates: An Experimental Study," Journal of Composites Technology & Research, 12(2): pp. 85-90.

[12] Somers, M., Weller, T. and Abramovich H., 1991. "Influence of predetermined delaminations on buckling and postbuckling of composite sandwich beams," Composite Structures 17, pp. 295-329.

[13] Hwu, C., and Hu, J.S., 1992. "Buckling and Post-buckling of Delaminated Composite Sandwich Beams," AIAA Journal, 30(7), pp.1901-1909.

[14] Lim, Y.B., and Parsons, I.D., 1992. "The linearized buckling analysis of a composite beam with multiple delaminations," International Journal of Solids and Structures 30(22), 3085–99.

[15] Suemasu, H., 1993. "Effects of multiple delaminations on compressive buckling behaviors of composite panels," Journal of Composite Materials 27(12), 1173–92.

[16] Chen, H.P., 1993. "Transverse shear effects on buckling and postbuckling of laminated and delaminated plates," AIAA Journal 31, pp.163–169.

[17] Yeh, M.K., and Tan, C.M., 1994. "Buckling of elliptically delaminated composite plates," Journal of Composite Materials 28(1), pp.36–52.

[18] Cheng, S.H., Lin, C.C., and Wang, T.S., 1997. "Local buckling of delaminated sandwich beams using continuous analysis," International Journal of Solids and Structures 34(2), pp. 275-288.

[19] Hwu, C., and Hsieh, C.H., 1998. "The effect of transverse shear stress on the buckling of the delaminated composite sandwich beams," The First Asian-Australasian Conference on Composite Materials, Osaka, Vol. I, pp.303.1-303.4.

[20] Zhang, X., and Yu, S., 1999. "The growth simulation of circular buckling-driven delamination," International Journal of Solids and Structures 36, pp.1799–1821.

[21] Li, D., Tang, G., Zhou, J., and Lei, Y., 2005. "Buckling analysis of a plate with built-in rectangular delamination by strip distributed transfer function method," Acta Mechanica 176, pp. 231–243.

[22] Sekine, H., Hu, N., and Kouchakzadeh, M.A., 2000. "Buckling analysis of elliptically delaminated composite laminates with consideration of partial closure of delamination," Journal of Composite Materials 34(7), 551–76.

[23] Yu, H.H., and Hutchinson, J.W., 2002. "Influence of substrate compliance on buckling delamination of thin films," International Journal of Fracture 113(1), pp. 39-55.

[24] Shu, D., and Parlapalli, M., 2004. "Buckling analysis of bimaterial beams with single asymmetric delamination," Composite Structures 64, pp. 501–509.

[25] Mahfuz, H., Islam, S., Saha, M., Carlsson, L., and Jeelani, S., 2005. "Buckling of sandwich composites; effects of core-skin debonding and core density," Applied Composite Materials12, pp. 73-91.

[26] Dost, E., F., Ilcewicz, L. B., Avery, W., B., and Coxon, B., R., 1991. "Effects of stacking sequence on impact damage resistance and residual strength for quasi-isotropic laminates," ASTM STP 1110, pp.476-500.

[27] Hitchen, S. A., and Kemp, R., M., J., 1995. "The effect of stacking sequence on impact damage in a carbon fibre/epoxy composite," Composite Structures, Vol.26 (3), pp.207-214.

[28] Xiong, Y., Poon, C., Straznicky P., V., and Vietinghoff, H., 1995. "A prediction method for the compressive strength of impact damaged composite laminates," Composite Structures, Vol.30, pp.357-367.

[29] Ishikawa, T., and Suemasu, H., 2002. "Clarification of mechanical behavior in compression after impact (CAI) and open hole compression (OHC) tests for carbon/polymer composites," Proceedings of the Tenth US-Japan Conference Composites Materials, Stanford, CA USA, pp.21-32.

[30] Suemasu, H., Osada Y., and Wakabayashi H., 2001. "Compressive behavior of composite laminates with different size multiple delaminations," Proceedings of the ICCM-13, Beijing, China, ID-1654.

[31] Davies, G., A., O., and Zhang, X., 1995. "Impact damage prediction in carbon composite structures". International Journal of Impact Engineering," Vol.16, pp.149-170.

[32] Soutis C. and Curtis, P., T., 1996. "Prediction of the post impact compressive strength of CFRP laminated composites," Composites Science and Technology, Vol.56, pp.677-684.

[33] Zhou, G. and Rivera, L. A., 2005. "Investigation for the reduction of in-plane compressive strength in preconditioned thin composite panels," Journal of Composite Materials, Vol. 39, pp.391-422.

[34] Rosenfeld, M. S. and Gause, L. W., 1981. "Compression Fatigue Behavior of Graphite/Epoxy in the Presence of Stress Raisers, Fatigue of Fibrous Composite Materials," American Society for Testing and Materials, Philadelphia, PA, ASTM STP 723, pp. 174_196.

[35] Ramkumar, R. L, 1983. "Effect of Low-velocity Impact Damage on the Fatigue Behavior of Graphite/Epoxy Laminates, In: Keven O'Brien, T. (ed.), Long-Term Behavior of Composites," American Society for Testing and Materials, Philadelphia, PA, USA, ASTMSTP 813, pp. 116_135.

[36] Griffin, C. F. and Becht, G. J, 1991. "Fatigue Behavior of Impact Damaged BMI and Thermoplastic Graphite Composites," In: Proceedings of the 36th International SAMPE Symposium, San Diego, CA, and 15_18 April, pp. 2197–2209.

[37] Ong, C. L., Sheu, M. F., Liou, Y. Y. , and Hsiao, T. J, 1991. "The Study of the Fatigue Characteristics of Composite after Impact," In: Proceedings of the 36th International SAMPE Symposium, San Diego, CA, 15_18 April, pp. 912–923.

[38] Swanson, S. R., Cairns, D. S., Guyll, M. E. and Johnson, D., 1993. "Compression Fatigue Response for Carbon Fiber with Conventional and Toughened Epoxy Matrices with Damage," Journal of Engineering Materials and Technology, 115(1), pp. 116_121.

[39] Mitrovic, M., Hahn, H. T., Carman, G. P. and Shyprykevich, P., 1999. "Effect of Loading Parameters on the Fatigue Behavior of Impact Damaged Composite Laminates," Composites Science and Technology, 59(14), pp. 2059_2078.

[40] Beheshty, M. H., Harris B. and Adam, T., 1999. "An empirical fatigue-life model for high-performance fibre composites with and without impact damage," Composites Part A (Applied Science and Manufacturing), vol.30A (8), pp.971-987.

[41] Symons, D. D. and Davis, G., 2000. "Fatigue Testing of Impact-damaged T300/914 Carbon fiber- reinforced Plastic," Composites Science and Technology, 60(3), pp. 379_389.

[42] Colombo C., Vergani, L., 2014 "Influence of delamination on fatigue properties of a fiberglass composite," Composite Structures, 107, pp.325–333.

[43] Chen, A. S., Almond, D. P. and Harris, B., 2001. "In Situ Monitoring in Real Time of Fatigue induced Damage Growth in Composite Materials by Acoustography," Composites Science and Technology, 61(16), pp. 2437-2443.

[44] Melin, L. G. and Schon, J., 2001. "Buckling Behavior and Delamination Growth in Impacted Composite Specimens under Fatigue Load: An Experimental Study," Composites Science and Technology, 61(13), pp. 1841-1852.

[45] Gower, M. R. L. and Shaw, R. M., 2008. "Assessment of the Applicability of Compression-After- Impact (CAI) and Open Hole Tension (OHT) Methods for Use Under Fatigue Loading," In: 13th European Conference on Composite Materials, Stockholm, Sweden.

[46] Uda, N., Ono, K. and Kunoo, K., 2009. "Compression Fatigue Failure of CFRP Laminates with Impact Damage," Composites Science and Technology, 69(14), pp.2308-2314.

[47] Kulkarni, N., Mahfuz, H., Jeelani, S., and Carlsson, L.A. (2003). "Fatigue Crack Growth and Life Predication of Foam Sandwich Composites under Flexural Loading,". Composite Structures, 59, pp.499–505.

[48] Freeman, B., Schwingler, E., Mahinfalah, M., and Kellogg, K. (2005). "The Effect of Low-Velocity Impact on the Fatigue Life of Sandwich Composites," Composite Structures, 70, pp. 374–381.

[49] Belingard, G., Martella P., and Peroni, L. (2007). "Fatigue analysis of honeycomb-composite Sandwich beams," Composites: Part A, 38, pp. 1183–1191.

[50] Soni, M. S., Gibson, R. F, and Ayorinde, E. O., 2008. "The Influence of Subzero Temperatures on Fatigue Behavior of Composite Sandwich Structures," Composite Sciences and Technology, 69, pp. 829-838.

[51] Bezazi, A., El Mahi, A., Berthelot, J.M., and Bezzazi, B. (2009). "Experimental Analysis of Behavior and Damage of Sandwich Composite Materials in Three-point Bending," Part 2. Fatigue Test Results and Damage Mechanism, Strength of Materials, Vol. 41, No. 3, UDC 539.4.

[52] Belouettar, S., Abbadi, A., Azari, Z., Belouettar, R., and Freres, P. (2009). "Experimental Investigation of Static and Fatigue Behavior of Composites Honeycomb Materials Using Four Point Bending Tests," Composite Structures, 87, pp. 265-273.

[53] Teixeira, F.S, Kolstein H., Bijlaard, F. "Fatigue behavior of bonded and sandwich systems for strengthening orthotropic bridge decks," Composite Structures 2013; 97, pp.117–128.

[54] Nettles, A., Hodge, A., and Jackson, J. 2011. "An Examination of the Compressive Cyclic Loading Aspects of Damage Tolerance for Polymer Matrix Launch Vehicle Hardware," Materials and Processes Laboratory, NASA Marshall Space Flight Center, AL, USA.

[55] Shyprykevich, P., Tomblin, J., Ilcewicz, L., Vizzini, A. J., Lacy, T. E. and Hwang, Y. 2002. "Guidelines for Analysis, Testing and Nondestructive Inspection of Impact-damaged Composite Sandwich Structures," Federal

Aviation Administration Report DOT/FAA/AR-02/121, Office of Aviation Research, Washington.

[56] Hwang W, S., Han, K., 1986. "Fatigue of composites-fatigue modulus concept and life prediction," Journal of Composite Materials; 20, pp. 155–65.

ABSTRACT

EFFECT OF IMPACT DAMAGE ON COMPRESSION-COMPRESSION FATIGUE BEHAVIOR OF SANDWICH COMPOSITES

by

ALI M. AL-SHARIF

May 2015

Advisor: Prof. Golam Newaz

Major: Mechanical Engineering

Degree: Doctor of Philosophy

The aim of this research work was to investigate the effect of impact damage on in-plane buckling and compression-compression fatigue behavior for a new sandwich structure made from E-glass/epoxy face sheets over end-grain balsa wood core. Low velocity impact tests were carried out using a drop-weight impact tower by impacting the sandwich beam at the center with energy level slightly higher than threshold energy level of 8.8 J. Edge-wise compression static tests were conducted for impacted and non-impacted samples to address energy absorption characteristics of these composites. Analytical and experimental investigations were carried out to measure critical buckling loads and study the response and failure modes of debonded composite sandwich beams under compressive loads. These composite sandwich beams with local delamination caused by low velocity impact were utilized to evaluate the compression fatigue performance. Compression-Compression fatigue tests were conducted for

specimens with and without impact damage. Compressive residual strengths were obtained and the growth of delamination was monitored during fatigue tests. Although fatigue performance was adversely affected due to the presence of impact induced damage, it was observed that delamination growth does not occur in fatigue for in-plane stress levels below 40% of compression-after-impact (CAI) values for this class of sandwich composites. Results showed that there was significant degradation of fatigue life due to impact damage in relation to undamaged composite. Also, it was observed that any appreciable stiffness loss in fatigue does not occur below 50% CAI value. The combined damage consisting of delamination, core shear and skin failure was found to be the dominant failure mode under compression fatigue. The finite element analysis (ABAQUS) was utilized to predict the interfacial stress and stress distribution along thickness of the undamaged composite beam. The normal compressive stress distribution along thickness was plotted. The results showed very good agreement for facing and core stress values obtained by the analytical and numerical solutions. The predicted interfacial stress value was found to be between the facing and core stresses. These micromechanics results provide a clear understanding of the local behavior and how they influence the overall composite behavior. A unique contribution of the thesis work is compressive fatigue response characteristics of glass fiber sandwich composites subjected to lateral impact. These results are likely to be integrated into design of lightweight decks in automotive and truck applications.

AUTOBIOGRAAPHICAL STATEMENT

ALI M. AL-SHARIF

Ali Mohamed Esmaeel Al-Sharif is currently Ph.D. candidate at Wayne State University and expects to graduate by this year 2015. Ali came to Wayne State University after several years of service to Sabha University in Libya. While there he taught various courses and supervised several undergraduate projects in the Mechanical Engineering Department. Before joining the Engineering School faculty at Sabha, he was a student at Budapest University of Technology and Economics in Budapest, Hungary. He applied for his Master's program in Mechanical Engineering and graduated in 2005. After earning his Bachelor's degree in Mechanical Engineering from Garyounis University in Libya, he also has served within the mechanical engineering discipline in Libya for several employers, including as Mechanical Engineering Supervisor at Tassli Office for Engineering Consultations, Mechanical Engineer at Alsharara Factory, and Mechanical Engineer under the Maintenance & Construction Departments at Alwaha Oil Company. He received scholarships to apply for both his Master's and Ph.D.'s degrees. He also received the Thomas C. Rumble University Graduate Fellowship from Wayne State for 2012-2013. Ali is a member in a variety of honor and engineering organizations such as The National Engineering Honor Society (Tau Beta Pi), Michigan Epsilon Chapter, Golden Key Honor Society, WSU Chapter, the Engineering Society of Detroit, Society of Plastic Engineers (SPE) and American Society of Mechanical Engineers (ASME), WSU Chapter.